



ELSEVIER

Contents lists available at ScienceDirect

# Quaternary Science Reviews

journal homepage: [www.elsevier.com/locate/quascirev](http://www.elsevier.com/locate/quascirev)

## Fires and rates of change in the temperate rainforests of northwestern Patagonia since ~18 ka

Patricio I. Moreno <sup>a, b, \*</sup>, César Méndez <sup>c</sup>, Carla A. Henríquez <sup>a, b</sup>, Emilia I. Fercovic <sup>a, b</sup>, Javiera Videla <sup>a, b</sup>, Omar Reyes <sup>c, d</sup>, Leonardo A. Villacís <sup>a, b</sup>, Rodrigo Villa-Martínez <sup>e</sup>, Brent V. Alloway <sup>f</sup>

<sup>a</sup> Center for Climate Research and Resilience, Universidad de Chile, Santiago, Chile

<sup>b</sup> Departamento de Ciencias Ecológicas, Universidad de Chile, Santiago, Chile

<sup>c</sup> Centro de Investigación en Ecosistemas de la Patagonia, Coyhaique, Chile

<sup>d</sup> Centro de Estudios del Hombre Austral, Universidad de Magallanes, Punta Arenas, Chile

<sup>e</sup> Centro de Investigación GAIA-Antártica, Universidad de Magallanes, Punta Arenas, Chile

<sup>f</sup> Instituto de Geografía, Pontificia Universidad Católica de Chile, Santiago, Chile



### ARTICLE INFO

#### Article history:

Received 21 July 2022

Received in revised form

22 November 2022

Accepted 28 November 2022

Available online 16 December 2022

#### Keywords:

Macroscopic Charcoal Accumulation Rates

Rates of vegetation change

Temperate rainforests

Northwestern Patagonia

Explosive volcanism

Human occupations

Southern westerly winds

Chilean/European settlers

### ABSTRACT

We examine the temporal and spatial structure of wildfires and rates of vegetation change in the Pacific sector of northwestern Patagonia ( $40^{\circ}$ – $44^{\circ}$ S) over the last ~18,000 years. Macroscopic Charcoal Accumulation Rates (CHAR), a proxy of past local fires, shows a geographic variation that mirrors the modern north-to-south and low-to-high elevation increase in annual precipitation and decrease in precipitation seasonality, and the frequency of explosive volcanic events. Variability in past fires is evident at multiple timescales, with a significant multi-millennial low between ~18–13.1 ka, an abrupt rise between ~13.1–12.5 ka, and heightened fire activity between ~11.4–8.2 ka with significant high values between ~10–9.4 ka. A subsequent decline led to the lowest Holocene values between ~6–5.4 ka, which rose and led to significant high values between ~3.1 ka and the present. Andean and Western Upwind Environments share a multi-millennial structure of fire activity since ~18 ka, overprinted by millennial and centennial-scale divergences. These differences underscore the role of explosive volcanism as a trigger or modulator of fire activity in the vicinity of Andean eruptive centers. We posit that fire activity in Western Upwind Environments was driven primarily by hydroclimate variations, namely changes in the intensity of the Southern Westerly Winds. Compilations of CHAR and the Rates of Change (ROC) parameter, a measure of the magnitude and rapidity of changes in the pollen records, covary during the onset of the interglacial fire regime at ~13.1 ka and the last ~4000 years, suggesting that fires catalyzed vegetation changes during specific intervals since the last glaciation. Highly mobile human occupations deployed along the coasts started at ~6.2 ka, increased in pulses, and spread widely during the last two millennia. Covariation with CHAR and ROC since ~4 ka suggests that hunter-gatherer-fishers contributed to enhanced fire activity and abrupt vegetation changes at regional scale. The ubiquitous fire maximum over the last four centuries relates to widespread settlement and associated large-scale land clearance conducted by European/Chilean settlers.

© 2022 Elsevier Ltd. All rights reserved.

### 1. Introduction

Wildfires have shaped the structure, composition, and functioning of nearly all terrestrial ecosystems at global scale, affecting

sedimentary and geomorphic processes (Kean et al., 2011), atmospheric chemistry (Galanter et al., 2000), radiative balance (Zhang and Wang, 2011) and the global Carbon cycle (Van Der Werf et al., 2004). The frequency, magnitude, and temporal/spatial structure of wildfires define the fire regime for any given area (Krebs et al., 2010). Fire regimes are expected to change during the 21st century as a consequence of climate change and anthropogenic pressure on the landscapes (Krawchuk et al., 2009). Hence, it is

\* Corresponding author. Center for Climate Research and Resilience, Universidad de Chile, Santiago, Chile.

E-mail address: [pimoreno@uchile.cl](mailto:pimoreno@uchile.cl) (P.I. Moreno).

important to improve our understanding of the linkages between climate, vegetation type, fire regimes, and non-climatic influences (explosive volcanism, human activities) to anticipate the potential consequences of future climate change, and for increasing societal preparedness and resilience (Cooper and Sheets, 2012).

Lake sediments from small closed-basin sites allow the development of continuous time series of past fires at relatively high spatial and temporal resolution, i.e., from decadal scale and a few km<sup>2</sup> surrounding the site. When carried out in conjunction with other environmental indicators, they enable the study of the reciprocal relationships between vegetation, fire, explosive volcanism, and climate, which can be compared with archaeological records at comparable spatial and temporal scales to examine the potential influence of human activities through space and time.

The narrow and intricate terrain of Patagonia between the Pacific coast and the continental divide established by the southern

Andes ridge (40°S–55°30'S, Fig. 1) is an interesting region to explore the linkages between past climate, vegetation, and fire regimes in the temperate, volcanically active zone of southern South America, and their likely evolution under future climate change scenarios. Large-scale fires in central/southern Chile (32°S–42°S) during recent years highlight the vulnerability of natural and managed landscapes to a widespread (and ongoing) megadrought (Garreaud et al., 2017; González et al., 2018; McWethy et al., 2021; Rick et al., 2020), with important repercussions for human welfare, biodiversity, and ecosystem services. The Pacific sector of northern and central Patagonia are key areas to examine these processes, considering the wealth of glacial, geological, palaeoecological, and archaeological studies (see section 1.2 titled “Glacier, vegetation, fire, climate, and human history in NWP since ~18 ka”), and the contrasts in timing and magnitude of human occupations in the mainland and archipelagos during historical and pre-Columbian

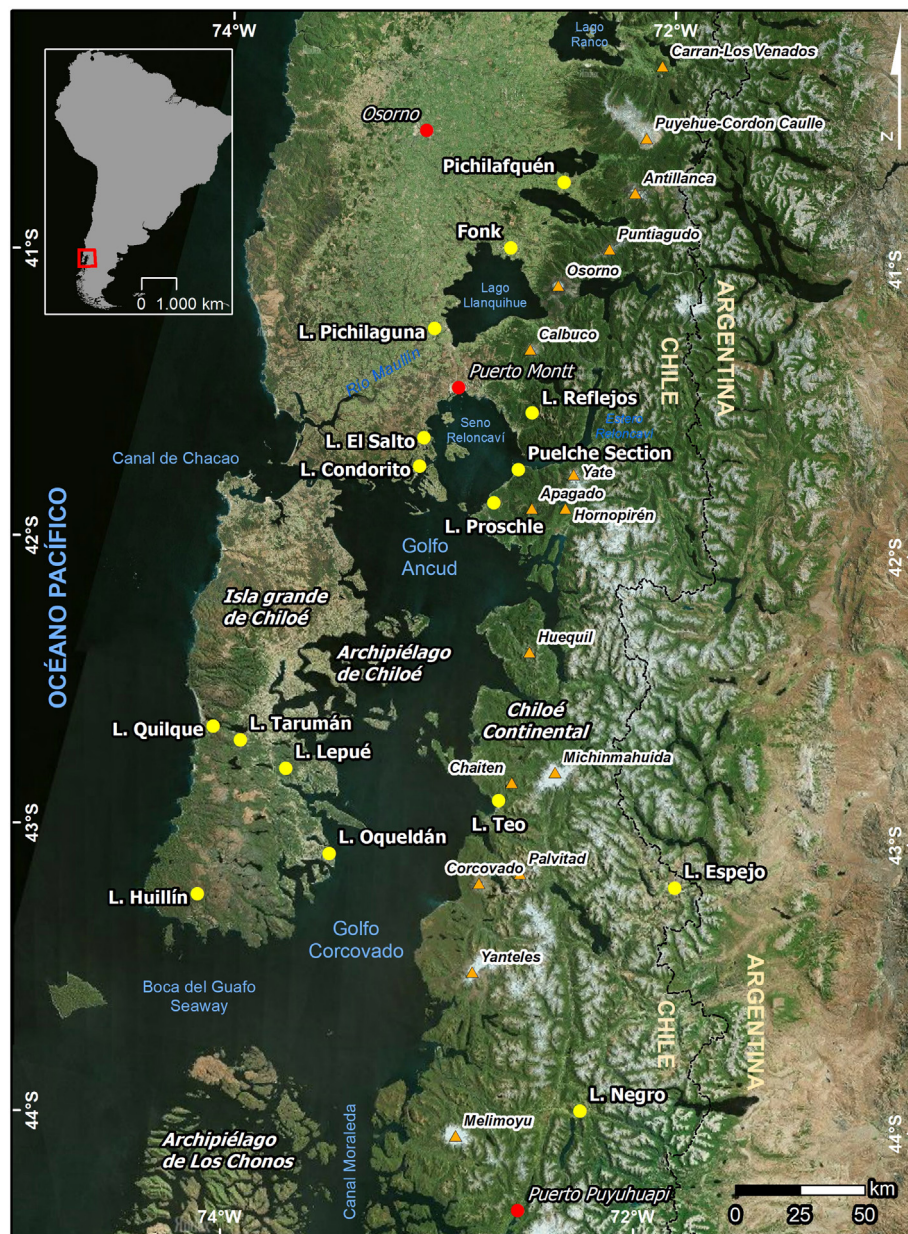


**Fig. 1.** Map of Northwestern Patagonia showing physiographic units and localities mentioned in the main text. The orange triangles and names in italics show the main volcanic centers in the region

times. Within this area, Archipiélago de los Chonos is the least disturbed by modern human activities and features biodiverse temperate rainforests that face important challenges by current and future human activities. Yet, the archaeological record indicates human presence since mid-Holocene times along the coasts of the mainland and islands (Reyes, 2020).

In this paper we examine the temporal and geographic trends in paleofires along environmental gradients on the Pacific sector of Northwestern Patagonia (= NWP: 40°S–44°S) (see Table 1 for all acronyms used in this study). Our assessment is based on fifteen high-resolution macroscopic charcoal records we developed using the same field and laboratory methods to maximize compatibility among datasets. These sites were selected primarily on the basis of their sound stratigraphic and chronologic control and, above all, the availability of multidecadal-scale resolution macroscopic charcoal records spanning uninterrupted until the present. In addition, we quantify and compile the rates of change in the terrestrial vegetation and the occurrence of volcanic ash layers using data from the same sites and sediment cores. We also developed a database of radiocarbon-dated archaeological sites from northwestern and central-western Patagonia to assess potential relationships of the human occupation with records of environmental change (Sandweiss and Quilter, 2012). These data allow the examination of the role of vegetation, climate, explosive volcanism, and human activity on wildfires since ~18 ka (ka = 10<sup>3</sup> calibrated years before 1950 CE), the identification of ecosystem responses, driving factors, gaps in current knowledge, and perspectives for future improvements. In this paper we assess the following questions: (i) Is there a consistent temporal fire activity trend in NWP since ~18 ka? (ii) How did fire activity vary along a north-south transect and Andean/Western Upwind Environments in the region? (iii) Are we able to distinguish unsynchronized localized eruption-induced fire activity from more regionally synchronous climate-induced fire activity? (iv) Did fire activity influence the rates of vegetation change (or vice versa) at regional scale? (v) How did fire activity vary in relation to changes in Southern Westerly Wind influence? and (vi) in relation to the temporal distribution of human occupations in the region?

**Table 1**  
Acronyms used in this study.

ACH	Archipiélago de los Chonos
AND	Andean
ANOVA	Analysis of Variance
CC	Chiloé Continental
CHACC	Charcoal Compilation Curve
CHAR	Charcoal accumulation rate
CLD	Chilean Lake District
DCA	Detrended Correspondence Analysis
DNC	Distance to the nearest eruptive center
DNE	Distance to the nearest coast
ECPI	<i>Eucryphia/Caldcluvia</i> to Podocarpaceae pollen Index
FL	Factor loading
IGC	Isla Grande de Chiloé
ka	10 <sup>3</sup> calibrated years before present, present = AD 1950
LGM	Last Glacial Maximum
masl	Meters above sea level
MST	Mean Spacing between Tephra
N+CP	Northwestern and coastal Central Western Patagonia
NWP	Northwestern Patagonia
RDA	Redundancy Analysis
ROC	Rates of Change
ROCC	Rates of Change Compilation Curve
RSD	Regime Shift Detection algorithm
SPD	Summed Probability Distribution
T1	Last Glacial Termination
TF	Tephra Frequency
TSA	Temperate South America
WUE	Western Upwind Environments

### 1.1. Study area and climate context

NWP includes a northern sector of the mainland, commonly known as the Chilean Lake District, the Archipiélago de Chiloé that includes about 40 islands, the largest and westernmost of which is Isla Grande de Chiloé, and the Chiloé Continental sector to the east. The latter corresponds to the Andes Cordillera rimmed by Golfo de Ancud and Golfo Corcovado to the west, commonly known as the Chiloé Interior Sea, and the Argentinean territory to the east (Fig. 1). The Chilean Lake District and Isla Grande de Chiloé feature the Cordillera de la Costa along their western edge, with a distinct north-to-south decline in elevation along a ~380 km axis. The coastal range features two major interruptions in this region: (i) a conspicuous ~100 km gap between latitudes 40°20'S and 42°06'S, with the prominent Río Maullín and Canal de Chacao, and (ii) a ~5 km-wide west-to-east oriented gorge at ~42°40'S occupied by Lago Cucao and Lago Huillinco in central Isla Grande de Chiloé. The landscape south of the Chilotan archipelago, in central-west Patagonia, features numerous channels, fjords, and over 150 scattered islands grouped in the Archipiélago de los Chonos between 43°45'S and 47°S. This archipelago is separated from Isla Grande de Chiloé in the north by the ~42-km wide Boca del Guafo seaway that connects Golfo Corcovado to the Pacific Ocean, and from the mainland by the north-south trending Canal Moraleda, the largest of the interior channels in Central-West Patagonia.

Glaciers occur on the highest Andean summits (2000–2800 masl), some of them large stratovolcanoes. Volcanism in this region results from the subduction of the Nazca Plate underneath the westward moving South American Plate (Stern, 2004), along a narrow volcanic arc that follows the Liquiñe-Ofqui fault system in Chile between 38°S and 46°S. The Southern Andean Volcanic Zone features at least 60 active or potentially active volcanoes in Chile and Argentina, as well as three caldera systems and numerous minor eruptive centers (Stern, 2004). Several volcanic centers in this region exhibit late Quaternary and historical activity (Alloway et al., 2007; Moreno et al., 2015a; Alloway et al., 2017a,b; Naranjo et al., 2017; Romero et al., 2021; Alloway et al., 2022) (Fig. 1), some of which have originated large explosive events, as recorded by tephra deposits along the western and, overwhelmingly, eastern flank of the NWP Andes. Sediment cores from small, closed-basin lakes in this region have detected multiple high-resolution record of explosive activity from multiple medial to distal Andean volcanic sources. These data feature a distinct increase in the number and thickness of pyroclastic deposits along a west-to-east axis, and in the vicinity of active volcanic centers. Published and ongoing studies, include comparisons with the cover-bed stratigraphy of volcanic deposits, confirm not only their volcanic origin but also the fallout nature of the vast majority of layers of pyroclastic material recorded in lake sediment cores, adding a valuable perspective for improving our understanding of the frequency and areal extent of past explosive volcanic events. Andisols (Soil Survey Staff, 2014) are well expressed in areas west of, and adjacent to, volcanic centers of the Cordillera de los Andes and extend down the Longitudinal Valley (Luzio et al., 2010; Casanova et al., 2013). Here, soil genesis is dominated by a flux of intermittently erupted Andean-sourced tephra which has continued to buildup soils at the ground surface separated by intervals where topdown weathering processes are intensified (Alloway et al., 2018). These andic soils typically form alternating layers of reddish-brown (Sr-) and yellowish-brown (Sy-) soil horizons preserved upon volcanic, glacial and fluvial landforms. The number of Sr- and Sy-horizons systematically increase with the age of the landforms they mantle and furthermore, have a clear implied connection to coupled glacial-interglacial climate cycles as indicated from palynological analysis of equivalent-aged

lake and bog sedimentary records retrieved from the Chilean Lake District (see Alloway et al., 2018 and references therein).

The present-day climate in the Pacific sector of NWP is temperate and wet, with mean annual temperatures ranging between 8° and 11 °C, along with mean annual precipitation between 1300 and 3500 mm/yr. Such large precipitation across NWP is caused by the frequent passage of extratropical weather systems embedded in the Southern Westerly Winds (SWW) that batter the Pacific coast. The forced uplift of moist-laden air masses over the coastal range of Chilean Lake District and Isla Grande de Chiloé causes local precipitation maxima in the upwind slopes and a weak but discernible rain shadow just to the east over the Chilean Lake District Longitudinal Valley and Chiloé Interior Sea (Fig. 1). The westerly winds then encounter the Austral Andes causing a marked precipitation maximum on the Chilean slopes -with values that can surpass 4000 mm/year- followed by a sharp transition to dry conditions (less than 400 mm/year) to the east of the Andes ridge into Argentinean Patagonia (Smith and Evans, 2007). Consistent with its advective nature, precipitation variability over western Patagonia is tightly coupled with the intensity of the incoming flow in the lower troposphere at synoptic, seasonal, and interannual time scales (Garreaud et al., 2013; Garreaud, 2007). During austral summer (December-January-February) the SWW is strongest, but its axis reaches its southern most position (>50°S) causing a slight relaxation of the westerly flow over northern Patagonia and the rest of central-southern Chile, while the opposite occurs during austral winter when westerlies reach their greatest strength. These changes result in a seasonal cycle of the precipitation (lower in summer, higher in winter) with an amplitude close to 25% of the annual mean across NWP (and a much larger seasonality farther north).

The austral summer not only brings a precipitation decline, but also higher air temperature, lower humidity, and enhanced insolation. Modern fires throughout the Pacific sector of western Patagonia tend to be constrained to spring and summer months with negative anomalies in precipitation (Holz et al., 2012; Urrutia-Jalabert et al., 2018), which in turn are caused by a weakening of the westerlies impinging the austral Andes (Garreaud et al., 2013). These anomalies are associated with interannual climate variability of tropical (El Niño-Southern Oscillation, e.g. Cai et al. (2020), Montecinos and Aceituno (2003), and extratropical origin (the Southern Annular Mode; Garreaud et al., 2013), which allow the desiccation of biomass in a vast region formerly dominated by temperate rainforests. We note that the Southern Annular Mode influence extends throughout western Patagonia, whereas the El Niño-Southern Oscillation influence is important in central Chile and fades south of ~45°S (Quintana and Aceituno, 2012). Decadal and centennial-scale climate variability generates conditions favorable for fire occurrence as well, according to tree-ring (Holz and Veblen, 2012) and high-resolution pollen records (Henríquez et al., 2021a; Moreno, 2020; Moreno et al., 2018b, 2021a; Moreno and Videla, 2016). Negative precipitation anomalies, associated with Southern Annular Mode positive states, in conjunction with continuous and abundant biomass, however, are necessary but insufficient conditions to account for the Holocene fire activity throughout NWP as the scarcity of natural ignition agents constitutes a limiting factor for wildfires. Ignition agents in the region fall in the climatic (lightning strikes) and non-climatic categories (volcanic and human).

Lightning strikes over the Pacific sector of western Patagonia occur despite the year-round atmospheric stability imparted by the SWW over the region, with clouds and precipitation of stratiform nature. A recent study examined the geographic, temporal, and synoptic context for lightning strikes using satellite, model, and reanalysis data between years 2005–2012 (Garreaud et al., 2014).

That analysis revealed a concentration of events during summer and autumn, associated with weak post-frontal convection just upwind of the westernmost orographic obstacles along the Pacific coast. Though limited in temporal scope to available instrumental records (for the objectives of our study) and lacking an analysis of the relationship between lightning strikes and local fires, the Garreaud et al. (2014) paper demonstrates that lightning strikes do occur in the temperate and hyper humid maritime region of western Patagonia in the modern climate, providing a potential ignition agent for wildfires.

Explosive volcanism can influence fire regimes by the direct incendiary effect of pyroclast deposition, or by generating significant volumes of dead biomass (litter, epiphytes, branches, tree trunks) by physical/chemical damage to the vegetation by volcanic ash fallout and acid aerosols (i.e., Puyehue-Cordón Caulle eruption of 2011, see Swanson et al., 2016). Recent studies have shown that sites located near explosive volcanic centers along the Pacific slope of NWP exhibit a statistically significant relationship between tephra deposition and local fires through the Holocene (Henríquez et al., 2015; Henríquez et al., 2021b; Jara et al., 2019). Furthermore, the paleovegetation records from those sites show a conspicuous predominance of fast-growth, early successional, shade-intolerant taxa favored by disturbance, establishing a contrast with the vegetation signal present in sites distal to the eruptive centers within the same climatic region (Moreno et al., 2021b).

Past human activity is capable of altering fire regimes, as well as the structure, composition, and dynamics of the local and regional vegetation (McWethy et al., 2013). This influence is expected to vary as a function of population density, technology, mobility, and its temporal persistence in the landscape, as long as vegetation and climate conditions are conducive for fire occurrence. Archaeological studies in NWP have documented hunter-gatherer occupations in the Chilean Lake District starting, conservatively, at ~14.6 ka (Dillehay, 1989), while in Isla Grande de Chiloé and Archipiélago de los Chonos the earliest dates approach ~6 ka (Reyes, 2020; San Román, 2014). Human presence since that age provides a potential source of ignition and a latent driver of fire-regime shifts in the region.

In closing this section, we note that Southern Annular Mode in austral summer-fall has exhibited a significant tendency towards its positive polarity during the last four decades (see Fogt and Marshall, 2020 for an updated review) causing a substantial decline in precipitation across NWP (e.g., Boisier et al., 2016; Garreaud, 2018). The positive Southern Annular Mode trend has been attributed primarily to the stratospheric ozone depletion but also to the increased atmospheric concentration of greenhouse gasses. Thus, the long-term decline in precipitation between 38°S and 45°S west of the Andes (including NWP) is one of the clearest manifestations of anthropogenic climate change in Chile (Boisier et al., 2016) and consistently projected to continue in the future (e.g., Aguayo et al., 2019) as the persistent increase in concentration of greenhouse gasses outweigh a potential recovery of the stratospheric ozone. This ongoing drying trend undoubtedly impacts the fire regime across NWP.

## 1.2. Glacier, vegetation, fire, climate, and human history in NWP since ~18 ka

NWP was covered by the Patagonian Ice Sheet during the Last Glacial Maximum (= LGM: ~35–18 ka). Piedmont glacier lobes extended west of Cordillera de los Andes into the lowlands, reaching the modern sea level from the latitude of Puerto Montt toward the southern end of the continent (Fig. 1). Mapping and radiocarbon dating of geomorphic features deposited by multiple piedmont glacier lobes from Lago Ranco (40°S) to Golfo de

Corcovado ( $43^{\circ}\text{S}$ ) constitute the basis for a regional glacial chronology (Denton et al., 1999; Soteres et al., 2022b). Available data indicate that these lobes achieved multiple maxima during the LGM and retreated toward the Andes, vacating the below sea-level portion of the Longitudinal Valley occupied by the rising Chiloé Interior Sea and large lake basins within the initial millennium of the Last Glacial Termination (= T1: ~18–12 ka) (Moreno et al., 2015b). Glacier cover through the final stages of T1 was limited, presumably confined to the highest Andean summits and valleys of southern Chiloé Continental (Davies et al., 2020; Palacios et al., 2020). A tacit assumption for the NWP region has been that glaciers retreated to their modern margins at the end of T1 and lingered with little variation until the present. More recently, Moreno et al. (2021b) and Soteres et al. (2022a) reported glacier readvances or standstills in the southern Chiloé Continental area under cold and humid conditions during the Antarctic Cold Reversal west and east of the divide in the core of the northern Patagonian Andes, respectively.

Palynological records from sites adjacent to the western LGM margins reveal a characteristic timing and structure of vegetation changes during T1 (Heusser, 1966; Heusser et al., 2006; Moreno, 2020; Moreno and Leon, 2003; Moreno et al., 2018a, 2022; Pesce and Moreno, 2014). Those records typically feature warming that led to a decline in Non-Arboreal Pollen between ~17.8–16.8 ka, dominated by cold-tolerant pioneer herbs and shrubs, along with increases in pioneer shade-intolerant trees (Henríquez et al., 2021a). High abundance of littoral macrophytes (*Isoetes*, Cyperaceae) in several sites between ~17.8–16.3 ka (Fig. 2) suggests low-lake levels driven by reduced precipitation during the earliest portion of T1. Arboreal diversification and densification under wetter conditions led to the establishment of Evergreen North Patagonian rainforests dominated by thermophilous shade-tolerant trees and vines by ~16.8 ka (note the decline in Non-Arboreal Pollen, Fig. 2). A subsequent increase in cold-tolerant hygrophilous conifers (Podocarpaceae) (Fig. 2) marks a shift toward colder/wetter conditions between ~14.8–12.8 ka, followed by rapid increments in shade-intolerant trees favored by disturbance (*Weinmannia trichosperma*) in response to a decline in precipitation and enhanced fire activity between ~12.8–11 ka (Henríquez et al., 2021a).

Summer-drought tolerant tree species characteristic of the Evergreen Valdivian Rainforest (e.g., *Eucryphia/Caldcluvia*) (Fig. 2) established and attained considerable abundance during the early Holocene (~11.5–7.8 ka) in the Chilean Lake District, forming closed-canopy forests in the northern sectors of Isla Grande de Chiloé and Chiloé Continental. The abundance of Evergreen Valdivian Rainforest trees fades southward, reaching minimum abundance at the southern limits of Isla Grande de Chiloé and Chiloé Continental (Moreno et al., 2021b). The ~11–7.8 ka interval features low lake levels in some NWP sites, as evinced by the % *Isoetes* maximum in Fig. 2, documenting a precipitation minimum during the early Holocene (Fig. 2). A vegetation shift started at ~7.8 ka with a decline in thermophilous Evergreen Valdivian Rainforest trees, an increase in generalist taxa common to this vegetation unit and the Evergreen North Patagonian rainforest, along with cold-tolerant hygrophilous conifers (Podocarpaceae) characteristic of the latter forest (Fig. 2), and a sustained decline in % *Isoetes* (Fig. 2). The abundance of cold-tolerant hygrophilous conifers is maximal in the southern maritime sites and decline northward to a minimum in the northernmost inland sites (Moreno et al., 2021b). Unlike the coastal sectors, the northern Chilean Lake District sites feature persistence and intensification of Evergreen Valdivian Rainforest dominance through the middle Holocene (~7.8–4 ka), which decline in abundance after ~4 ka (Henríquez et al., 2021b; Moreno et al., 2021b). The remaining sites feature gradual mixing of

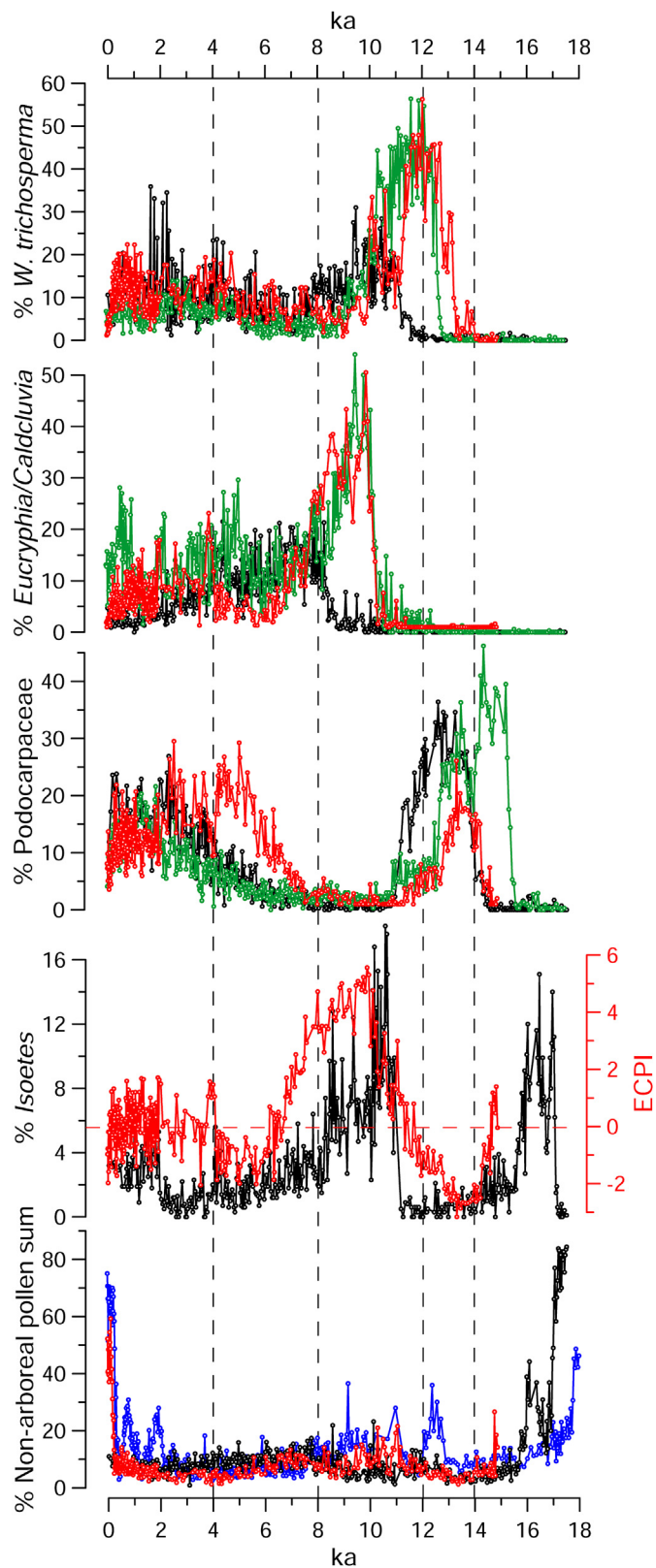


**Fig. 2.** Selected palynomorphs from sites located in Northwestern Patagonia (black: L. Lepué, green: L. Proschie, blue: L. Pichilaguna, red: the *Eucryphia/Caldcluvia* to Podocarpaceae pollen Index from Lago Condorito (ECPI)). The dashed red horizontal line marks the mean of the ECPI series. The ECPI from L. Condorito and the % *Isoetes* from Lago Lepué curves are also shown in Fig. 9, the % non-arboREAL pollen sum from L. Pichilaguna is also shown in Fig. 10. (For interpretation of the references to colour in this figure legend, the reader is referred to the Web version of this article.)

Evergreen Valdivian Rainforest and Evergreen North Patagonian Rainforest elements after ~7.8 ka, overprinted by millennial and centennial-scale fluctuations. Disturbance by European/Chilean settlers since ~0.35 ka caused rapid deforestation, illustrated by a rapid increase in Non-Arboreal Pollen (Fig. 2), resulting from the use of fire for land clearance and conversion to pastoral farming. The *Eucryphia/Caldcluvia* to Podocarpaceae index from Lago Condorito captures multi-millennial scale changes in hydrologic balance near the southern coast of the Chilean Lake District since ~14 ka (Fig. 2). Positive anomalies correspond with dominance of Evergreen Valdivian Rainforest trees under relatively warm and dry conditions during the early Holocene, bounded by values around the mean or negative anomalies with abundant Evergreen North Patagonian Rainforest conifers during the ~14–11 ka and ~7–4 ka intervals, implying relatively cold-wet conditions. The most recent ~4000 years feature values around the mean, indicating an intermediate condition with frequent, low-magnitude oscillations.

Some palynological studies from the Pacific sector of western Patagonia have utilized the Rates of Change (ROC) parameter as a measure of the magnitude, rapidity, and variability of the former vegetation. Increments in ROC have been shown to correspond with proxies of climate change (Moreno, 2004; Moreno et al., 2015b, 2018a), disturbance (Henríquez et al., 2021b; Moreno, 2020; Villa-Martínez and Moreno, 2021), and forest succession (Moreno and Leon, 2003). To date, however, no studies have examined the spatial and temporal trends in ROC at the landscape and regional scale in the Pacific sector of western Patagonia. Recently, Mottl et al. (2021a) developed and discussed a series of continental-scale compilations of rates of vegetation change using pollen data downloaded from the Neotoma database. Those authors detected a global acceleration in ROC between ~4.6–2.9 ka, with important differences at subcontinental scale. In the case of “temperate South America” they utilized 17 records spread along ~2100 km between ~37°S and 55°S east of the Patagonian Andes, half of which were derived from bogs and fens. Within this region, Mottl et al. (2021a) found a gradual and steady decline in ROC from ~18 ka to ~3 ka, followed by a modest and gradual increase toward the present.

Regional syntheses of fossil charcoal data throughout Patagonia includes records retrieved from lakes, bogs, and littoral/paludal environments in the periphery of lakes (Huber et al., 2004; Power et al., 2008; Whitlock et al., 2007). One caveat of peat records, however, is that peat accumulation/decomposition is intermittent and spatially variable throughout the bog/fen surfaces, and they yield charcoal records strongly skewed toward a local or azonal signal blurring the interpretation of extra-local or watershed-scale fire regimes. The most recent continental-scale charcoal synthesis (Power et al., 2008) combined charcoal records throughout Chile and Argentina to produce a summary anomaly curve for southern South America >30°S, i.e., from subtropical to sub-Antarctic environments west and east of the Andes Cordillera. The charcoal database features sites with large heterogeneities in analytical methods and laboratory techniques, quality contrasts in stratigraphic and chronologic control, and differences in the quantification of charcoal abundance, precluding direct comparisons among individual records. Although artificial, compatibility for all data types was possible through rescaling, normalization, and standardization of individual series, followed by interpolation at regular time intervals under the assumptions of depositional continuity and fire-regime constancy. Despite these shortcomings, the available syntheses allow examination of fire-regime changes at sub-continent and millennial scales and establishing comparisons with other landmasses. Taken at face value, available syntheses indicate that fire activity was highest during the early Holocene, east and west of the Andes, followed by a decline during the middle

Holocene, and a spatially variable and modest increase during late Holocene time (~4–0 ka) (Power et al., 2008; Whitlock et al., 2007).

Past changes in vegetation and fire activity in NWP point to a severe multi-millennial warm/dry phase during the early Holocene, driven by zonally symmetric weakening of the SWW (Fletcher and Moreno, 2012). This extreme interglacial condition was followed by an increase in precipitation and decline in temperature at ~7.8 ka, brought by stronger SWW. Studies from NWP (Henríquez et al., 2021b; Moreno, 2020; Moreno and Videla, 2016) and southwestern Patagonia (Moreno et al., 2018b) reported the onset of centennial-scale variability beginning between ~6.3 ka and ~5.8 ka, respectively, that drove shifts in the structure and composition of the vegetation, lake-level declines, and enhanced fire activity during warm/dry intervals which were interpreted by Moreno and Videla (2016) as centennial-scale megadroughts.

Although archaeological records in NWP predate the Holocene, it is within this timeframe that widespread human presence becomes evident throughout southern South America (Méndez, 2013; Perez et al., 2016). The initial human presence on the lowlands of the southern Chilean Lake District has been described for two localities. Findings from Monte Verde date back to ~18.5 ka and have been suggested as the earliest human presence in the region (Dillehay, 1989; Dillehay et al., 2015). The evidence from these sites is described as a series of discontinuous and discrete occupational surfaces (or horizons), where a significant diversity of artifacts, organic evidence, remains of extinct fauna, and features have been preserved by exceptional conditions (Dillehay et al., 2015, 2019). Pilauco, the other lowland locality, is described as a paleontological/archaeological site, which has yielded evidence of extinct fauna in stratigraphic association with artifacts with ages as early as ~15.9 ka (Pino and Astorga, 2020). Most archaeological sites in the region, however, postdate this initial presence and show that mobile hunter-gatherers occupied the Holocene landscapes in the Chilean Lake District until ~1.7 ka, when the introduction of horticulture and pottery correlates with a reduction in mobility (Adán et al., 2016). While terrestrial mobility was dominant in continental areas (Chilean Lake District and Chiloé Continental), navigation was mandatory for the colonization of Archipiélago de Chiloé and A. de los Chinos by canoe hunter-fisher-gatherers until historical times (Reyes et al., 2015). Recent studies have synthesized and analyzed the distribution of radiocarbon-dated archaeological sites along western Patagonia (Campbell and Quiroz, 2015; Reyes et al., 2019a). Those analyses reveal an overwhelming dominance of coastal over inland archaeological sites in NWP, and insular sites over continental locations in the coast of Central-West Patagonia. The majority of records indicate occupations younger than ~6.2 ka. These are primarily shell-midden deposits produced by campsite activities of maritime-adapted peoples as indicated by their specialized technology, subsistence preferences, and dietary composition (Reyes, 2020; Labarca et al., 2021).

The potential relationship of past human activity with vegetation and fire-regime shifts has been examined at site-specific (Méndez et al., 2016; Moreno, 2000; Moreno and Leon, 2003) and regional scales throughout Patagonia (Heusser, 1994; Horta et al., 2019; Iglesias and Whitlock, 2014; Marcos et al., 2021; Markgraf and Anderson, 1994; Nanavati et al., 2019). We note a conspicuous dearth of analyses of this potential relationship at the landscape level and sub-millennial timescales (Moreno et al., 2001, 2018c; Nanavati et al., 2022), which is unsurprising considering the requirements for a dense array of detailed fire history and archaeological records to detect spatial/temporal anomalies within the same vegetation and climate zone.

## 2. Methods

We retrieved the entire sedimentary sequence from the central sector of fourteen small closed-basin lakes (Fig. 1, Supplementary Table 1), using short cores that preserve the delicate water-sediment interface and long cores for the deeper portions with Livingstone or UWITEC piston corers. One additional site (Puelche Section) is a stratigraphic section exposed during a public works widening of a road near Caleta Puelche. We interpret that these sediments were deposited in a small pond that developed in an intermrainal depression alongside Seno Reloncaví and terrestrialized during the most recent millennia. All sediment samples were stored at 4°C at the Quaternary Paleoecology Laboratory of Universidad de Chile. We obtained X-radiographs of the cores to document the stratigraphy and potential stratigraphic structures, measured the magnetic susceptibility with a Bartington MS3 point sensor at 1 cm resolution, and subsampled for loss-on-ignition (LOI, 1 cc), pollen (1 cc) and macroscopic charcoal (2 cc) analyses at 1 cm resolution following standard protocols (Faegri and Iversen, 1989; Heiri et al., 2001; Whitlock and Anderson, 2003).

We use the ash density data following the 925°C combustion (LOI<sub>925</sub>) as a proxy for siliciclastic sediments, which allow detection of tephra layers and clastic pulses as short-lived increases along the sedimentary sequence, clearly visible in the X-radiographs as dense layers having sharp upper and lower contacts. In two sites we used the bulk magnetic susceptibility (MS) of the sediments as a proxy for clastic and tephra layers, which normally shows a close correspondence with the siliciclastic density. In our experience, clastic peaks from lake sediment cores obtained from closed-basin sites at water depths >8 m are a good approximation to tephra fallout events throughout NWP. We have found, however, that these analyses at 1-cm resolution tend to underestimate the total number of tephra, considering that several layers are <1 cm thick. We acknowledge that non-volcanic or non-tephra fallout clastic layers also generate peaks in the LOI and MS data series in some records, however, these represent a minority of the total number of clastic peaks considering the site and core types, and coring depths we studied. In addition, we conducted visual inspection and geochemical characterization to validate the occurrence of tephra interbeds, i.e., Moreno et al. (2015a). We applied a CharAnalysis (Higuera et al., 2009) deconvolution of the LOI and MS data series to aid in the detection of statistically significant inorganic peaks, and for calculating their frequency/periodicity variations in each site.

The chronology of each sedimentary record is constrained by AMS radiocarbon dates obtained from bulk organic or plant macrofossil samples retrieved from 1-cm-thick sections throughout the cores. We developed Bayesian age models using the Bacon package (v2.5.8; Blaauw and Christen, 2011) for R and the SHCal20 radiocarbon calibration dataset (Hogg et al., 2020). The age models consider the instantaneous deposition of pyroclastic levels by subtracting the thickness of all tephra layers thicker than 1 cm. This tephra-free depth scale was also applied to the charcoal, palynology, LOI and MS data.

We tallied macroscopic charcoal particles (>106 mm) from continuous contiguous 1-cm thick sections throughout the cores, following careful sieving to avoid rupture of individual particles. The analyses were performed under a Zeiss KL1500 LCD stereoscope, and the abundance of macroscopic charcoal is expressed as Charcoal Accumulation Rates (CHAR) (particles\*cm<sup>-2</sup>\*year<sup>-1</sup>).

We calculated the Rates of Change (ROC) parameter starting from the raw pollen counts of terrestrial plant taxa with the aid of the R-Ratepol package for R (v1.0.0; Mottl et al., 2021b) for R (v4.2.1; R Core Team, 2022). The package allows for a standardization through grain-count randomization, which we set to 300 grains, and iterated the ROC parameter computation 1000 times.

This computation involves the transformation to percentage abundance data, a Grimm method smoothening (restricted to a minimum of 5 and a maximum of 9 adjacent samples that must comply with a maximum age range of 500 years), interpolation using moving windows of 250 years with 5 superimposed window shifts, and standardization of the resulting chord distances by 250 years. The resulting chord distance/time (ROC parameter) is a dissimilarity coefficient that quantifies the magnitude and rapidity of changes between adjacent samples in the pollen dataset, allowing examination of the abruptness or graduality of past shifts in the terrestrial vegetation.

We carried out a linear Redundancy Analysis using CHAR and selected pollen taxa abundances averaged over the last ~1000 years as response variables regressed upon climate variables (i.e., CR2\_met regional climate simulation [accessed 2/27/2021], Boisier et al., 2018), mean time spacing between tephra, and distance to the nearest coast and eruptive center, as explanatory variables. This allows us to examine the correlations amongst climatic, geographic, and biological variables on canonical ordination axes. Variables were checked for normality, normalized (by logarithmic or exponential transformation) if needed, and standardized before computing. This analysis excluded a site located just east of the Andean Divide of northern Chiloé Continental (Lago Espejo), as this is an outlier in various climate parameters. We also performed a Detrended Correspondence Analysis fed with LOI<sub>925</sub>, MS, and CHAR data, preprocessed with CharAnalysis (Higuera et al., 2009) to detect peak frequency over 4000-year time frames in the former and Box-Cox transformation in the latter, followed by standardization and minmax rescaling. This allows us to examine broad scale patterns in fires and tephra frequency, a proxy of explosive volcanism, and their potential covariation during the last ~12,800 years, which is the time period where all sites, except Lago Teo (excluded for this analysis), have data. This analysis also excludes Puelche section because of slumping of reworked clastic material in the upper section. The Redundancy Analysis and Detrended Correspondence Analysis were computed with the vegan package (v2.6–2; Oksanen et al., 2019) for R (v4.2.1; R Core Team, 2022).

We generated CHAR and ROC compilation curves on our NWP data with the aid of the paleofire (v1.2.4; Blarquez et al., 2014) package for R (v4.2.1; R Core Team, 2022), and established comparisons with publicly available data from the Global Paleofire Database accessible through the GCD package (v4.0.7; Blarquez et al., 2014). Prior to the development of summary curves, each individual CHAR and ROC series was submitted to a three-step data transformation protocol (Power et al., 2008) which involves min-max data-rescaling, normalization via Box-Cox transformation, and standardization to Z-scores. The base period selected for Z-score standardization was 12–0 ka. We then generated synthesis curves through a robust LOWESS procedure (Daniau et al., 2012), using 50-year prebinning windows, 100-year local fitting windows, and regular 50-year interpolations, in addition to 1000 bootstrap iterations. We performed a circular block bootstrap procedure with 1000 iterations to reveal significant local minima/maxima that surpass the 95% confidence interval of the composite time series. We report all values exceeding this confidence interval as significantly high or low values. We tested the significance of non-overlapping time windows in group-specific datasets of standardized CHAR and ROC series through T1 (~18–14 ka and ~14–12 ka) and the Holocene (early: ~12–8 ka, middle: ~8–4 ka, and late: ~4–0 ka) using a Kruskal ANOVA.

Compilation curves for each NWP sector are composed of 5 individual series, i.e., the Chilean Lake District includes Lago Pichilafquén, L. Fonk, L. Pichilaguna, L. El Salto, and L. Reflejos; Isla Grande de Chiloé includes L. Quilque, L. Tarumán, L. Lepué, L. Oqueldán, and L. Huillin; and Chiloé Continental includes L.

Proschle, Puelche Section, L. Espejo, L. Teo, and L. Negro ([Supplementary Table 1](#)). We then generated the Northwestern Patagonian, the Western Upwind Environments, and the Andean macroscopic Charcoal and Rates of Change compilations following the same procedure. For comparison purposes, we developed a Temperate South American Charcoal Compilation by accessing the Global Paleofire Database and selecting all Patagonian sites between latitudes 40°S and 60°S each having at least 5 radiocarbon-dated levels (19 sites total).

The inventory of radiocarbon dates from archaeological sites relies on published studies west of the Andes between 40°S and 46°S. This compilation involved the use of chronometric hygiene, as well as data quality control ([Bird et al., 2022](#)). Particularly, we discarded radiocarbon dates with large analytical errors ( $1\sigma > 150$  years) and with uncertain stratigraphic relationship with the occupational levels and anthropogenic evidence. We averaged radiocarbon dates at the site level to avoid the temporal bias imposed by the overrepresentation of intensely dated archaeological contexts in the cumulative probability curves. This was performed whenever two or more dates were statistically indistinguishable at a 95% confidence limit ([Ward and Wilson, 1978](#)). Combined dates are considered as minimum occupational events at a site-specific level ([Méndez, 2013](#)). The inventory of radiocarbon-dated archaeological sites is only considered representative for the Archipiélago de los Chonos because it was based on a research program intended to measure the temporal distribution of human activity across the area, and thus considered dating all available archaeological evidence minimizing biases in the construction of chronology ([Reyes et al., 2019a](#)). The datasets for the Chilean Lake District and Isla Grande de Chiloé are based on the cumulative work of different research teams over time and represent site-based studies and efforts other than systematic regional research, and hence, are less representative of the trajectories across time.

We calibrated radiocarbon dates at  $2\sigma$  using the SHCal20 curve for terrestrial samples and the Marine20 curve for marine samples ([Heaton et al., 2020](#); [Hogg et al., 2020](#)) included in the Rcarbon package (v1.4.2; [Crema and Bevan, 2021](#)) for R. We applied a correction of  $141 \pm 43$  years to marine samples from Chilean Lake District and Isla Grande de Chiloé, considering local reservoir age determinations, and a correction of  $52 \pm 47$  years to marine samples from Archipiélago de los Chonos ([Merino-Campos et al., 2019](#)). Radiocarbon dates from human bone samples collected from coastal sites were also corrected for marine reservoir-age effects, considering that their stable isotopic composition ( $\delta^{15}\text{N}$ ,  $\delta^{13}\text{C}$ ) suggested a diet 80% based on marine resources ([Reyes et al., 2019a,b](#)). Whenever isotopic data were not available ( $N = 4$ ; 8.3% of dated human remains), we assumed a terrestrial diet and hence no reservoir-age effect.

We calculated the summed probability distribution (SPD) of radiocarbon dates from archaeological sites from NWP and coastal Central Western Patagonia using the Rcarbon package (v1.4.2) for R, and developed compilation curves for Chilean Lake District, Isla Grande de Chiloé, Archipiélago de los Chonos, and Central-West Patagonia. Preprocessing involved hierarchical aggregation using the *binPrep* function set with 50-year bins to enable comparability between sites and variables. SPDs of radiocarbon dates have been extensively used as proxy of past human population levels based on the assumption that human activity produces datable material and that variability in dates is related to the human activity intensity in the landscape ([Crema and Bevan, 2021](#)), and hence relatable to fluctuations in the environment ([Rick, 1987](#); [Timpson et al., 2021](#); [Williams, 2012](#)).

### 3. Results

The fire history sites are spread throughout a ~65,000 km<sup>2</sup> region, from sea level to 800 m. a.s.l., along a ~360 km north-south axis (40°44'S-43°58'S) through a ~180 km west-east transect from the Pacific coast to the Andean divide (74°7'W-71°51'W) ([Fig. 1](#)). On average the Chilean Lake District sites are located ~37.1 km (min: 0.1 km, max: 90 km) from the nearest coast and ~32.5 km (min: 8.5 km, max: 116.4 km) from the nearest volcanic center ([Supplementary Table 1](#)). In the case of sites from Isla Grande de Chiloé the mean distances are ~7.7 and ~95.6 km, and in Chiloé Continental these are ~30.5 and ~30.5 km, respectively. The macroscopic CHAR records have a mean time resolution of 30 years between levels (min: 14, max: 55) and, as will be discussed in the following sections, come from sites that feature a variable number of tephra layers (min: 2, max: 30). The latter factor affects the Tephra Frequency (TF) and Mean Spacing between Tephra (MST) for each record.

A Redundancy Analysis (RDA) applied to variables related to modern climate for each site located west of the Andean divide ([Fig. 3](#)), along with their distance to the nearest coast (DNC), distance to the nearest eruptive center (DNE), and MST as explanatory variables, yielded a RDA Axis 1 that accounts for 37.9% of the variance with major contributions from mean summer temperature (factor loading [FL]: -0.8), mean annual temperature (FL: -0.76), annual precipitation (FL: 0.54), and percent summer precipitation (FL: 0.32). RDA Axis 2 accounts for 25.3% of the variance, with major contributions from DNE (FL: -0.74), MST (FL: -0.56), mean summer temperature (FL: 0.4), and annual precipitation (FL: 0.39). Together, RDA Axes 1 and 2 account for 63.2% of the total variance. The FL magnitude for the response variables is highest for CHAR (-0.74) and *Nothofagus* (0.4) along RDA Axis 1, and *Rumex* (0.66), *Plantago* (0.59), and *Eucryphia/Caldcluvia* (0.55) along RDA Axis 2.

A Detrended Correspondence Analysis (DCA) applied to the raw CHAR and TF time series younger than ~12.8 ka ([Fig. 4](#)) features an Axis 1 that accounts for 43.7% of the variance, with major contributions from L. Oqueldán TF (FL: 2), L. Lepué TF (FL: 2), L. Quilque TF (FL: 2), L. Proschle TF (FL: -2.6), L. Pichilaqué TF (FL: -1.8), and L. Fonk TF (FL: -1.6). We note stability of strong positive scores between ~12.8–8 ka along DCA Axis 1, a sustained trend toward negative values between ~8–4.9 ka and stability of strong negative values between ~4.9–0 ka. Axis 2 accounts for 15.4% of the variance, with major contributions from L. Pichilaqué TF (FL: 2), L. Fonk TF (FL: 1.9), L. Huillin TF (FL: 1.8), L. Negro CHAR (FL: -2), L. Pichilaguna TF (FL: -1.9), and L. El Salto TF (FL: -1.4). DCA Axis 2 scores remain close to zero between ~12.8–8.7 ka, change toward modest positive values between ~8.7–6.8 ka, increase to strong positive values until ~5.4 ka and start a sustained decline until the present, with an irreversible transition from positive to negative scores at ~2.9 ka. Together, Axes 1 and 2 account for 59.1% of the total variance. We observe a conspicuous segregation of samples by age along DCA Axis 1, with the oldest samples on the far right (~12.5–8.8 ka), shift toward the center along the upper right quadrant with samples aged between ~8.8–6.2 ka, continue to the upper left quadrant with samples ranging in age between ~6–2.9 ka, and finally shift to the lower left with samples younger than ~2.9 ka.

In the following sections we describe the time evolution of CHAR, clastic sediment content, and the ROC parameter from each physiographic and climatic sector of NWP defined in the introduction ([Supplementary Figs. 1, 3, 4, Supplementary Table 1](#)).

#### 3.1. Chilean Lake District

This sector features four lowland lakes spread along a ~110 km

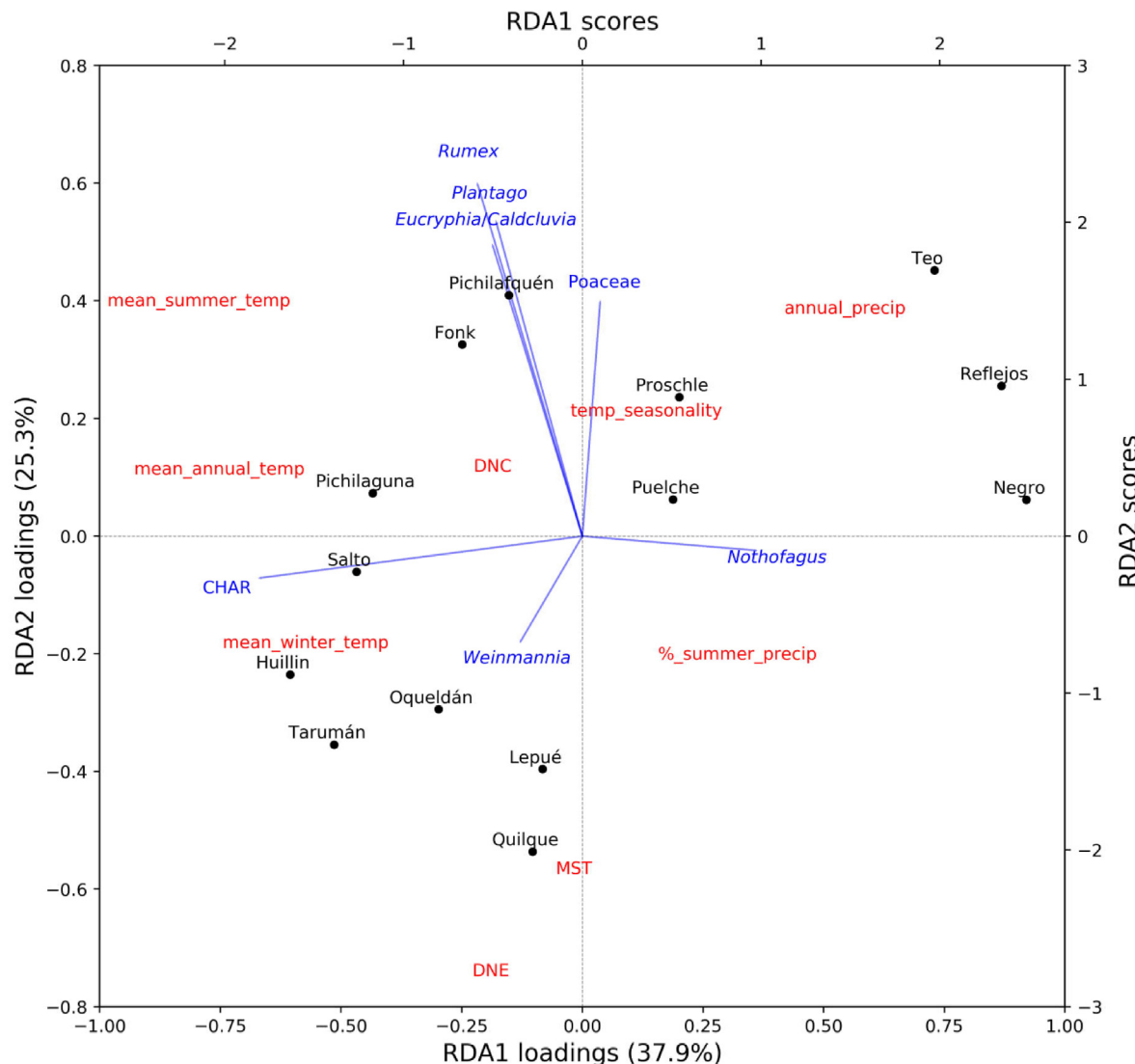


**Fig. 3.** Redundancy Analysis triplot of macroscopic charcoal records and selected pollen taxa from Northwestern Patagonia spanning the last millennium in the context of environmental variables related to geographic and climatic attributes, and mean time spacing between tephra.

north-south transect and a lake located on an Andean cirque (~800 m asl) at its southernmost sector, ~10 km north of the Seno Reloncaví coast (Fig. 1). The macroscopic charcoal compilation curve from sites located in the Chilean Lake District (CLD\_CHACC) (Fig. 5, Supplementary Fig. 1, Supplementary Table 1) reveals significant negative macroscopic CHAR values between ~18–13.5 ka, a modest rise that stabilizes at intermediate low values between ~13.5–12.9 ka, and a major peak between ~12.9–12.4 ka that surpasses the mean of the time series. A sharp decline takes place between ~12.4–12 ka, followed by a recovery culminating at ~11 ka. We observe predominance of positive anomalies between ~11.2–8.1 ka, with significant high levels between ~10–9 ka. Values decline to persistently negative anomalies between ~8.1–3.3 ka with the lowest numbers between ~6–5.4 ka and a positive anomaly peak between ~4.5–4.2 ka. Permanent positive anomalies prevail between ~3.3 ka and the present, with significant high values between ~1.2–0.8 ka and ~0.25–0.15 ka. Period-wise Kruskal ANOVAs (Supplementary Fig. 2) indicate that within the CLD\_CHACC dataset: ~12–8 ka = ~4–0 ka > ~8–4 ka > ~14–12 ka > ~18–14 ka.

The siliciclastic sediment density and magnetic susceptibility

data from sites located in the Chilean Lake District (Supplementary Fig. 1), aided by a peak detection algorithm, show abundant clastic peaks  $\geq 1$  cm thick we interpret as tephra layers. We detect 27 tephra layers in L. Pichilarquén since ~14.8 ka, followed by L. Fonk (27 layers since ~17.6 ka), and a significantly lower number in L. Pichilaguna (6 layers since ~18 ka) and L. El Salto (6 layers since ~15.3 ka). The siliciclastic density data from L. Reflejos shows an intermediate number of tephra (13) since ~16.3 ka.

The compilation curve of ROC records from sites located in the Chilean Lake District (CLD\_ROCC) (Fig. 5) shows predominance of significant low values between ~18–16.7 ka, punctuated by a prominent increase that leads to a positive anomaly peak at ~17.7 ka, and followed by a rise and increased variability interval between ~16.7–13.2 ka. Persistent positive anomalies prevail between ~13.2–11.8 ka with significant high values between ~12.4–11.9 ka. Millennial-scale oscillations around the mean dominate the record between ~11.9–4.5 ka, superseded by a steady rise that starts in modest negative values and culminates with significant high values between ~0.4 ka and the present. The Kruskal ANOVA analysis on the CLD\_ROCC dataset (Supplementary Fig. 2) indicates that (~14–12 ka > ~12–8 ka) = ~4–0 ka > ~8–4 ka > ~18–14 ka.

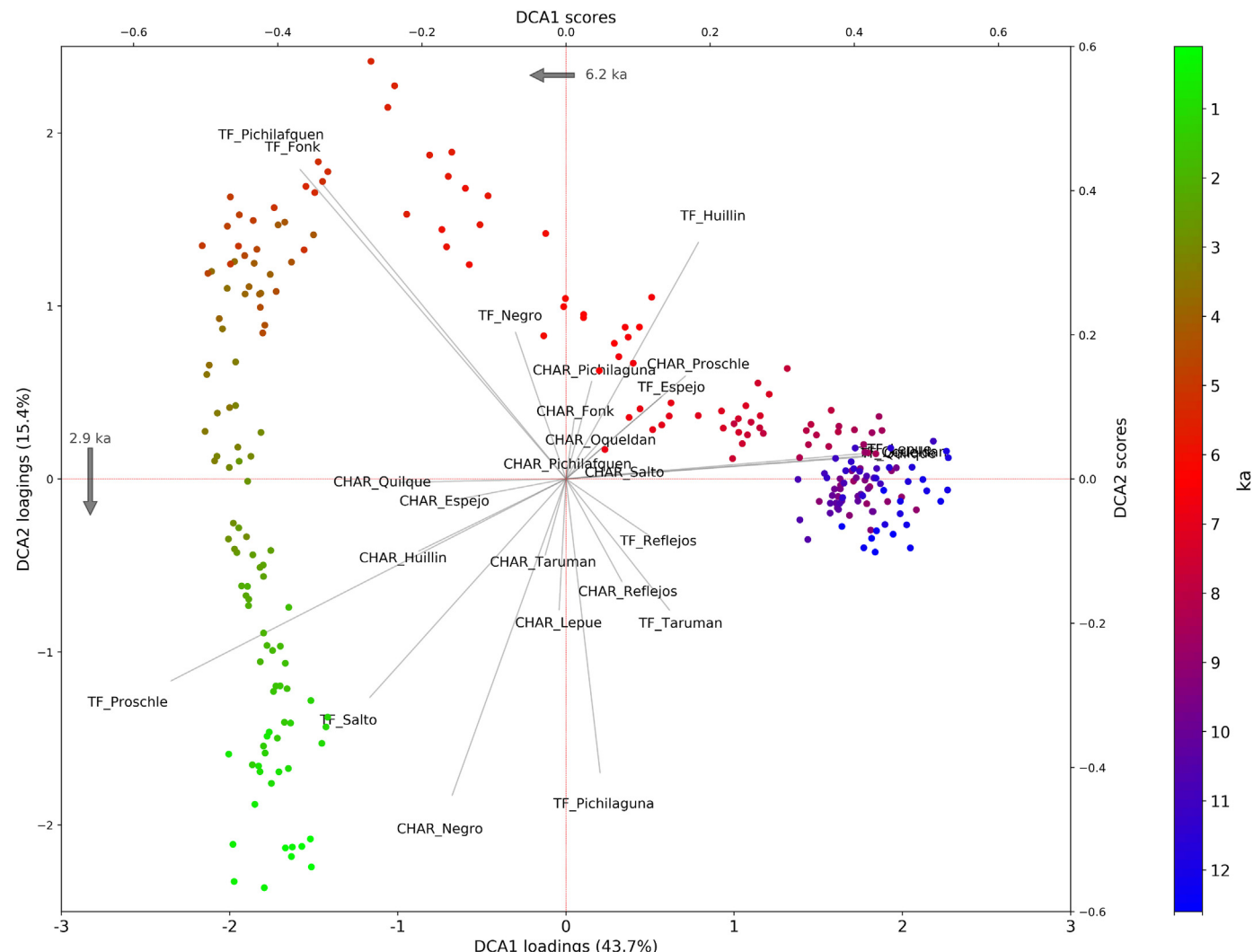


**Fig. 4.** Detrended Correspondence Analysis biplot of the macroscopic charcoal (CHAR) and tephra frequency (TF) time series.

We detect a weak correlation between CLD\_CHACC and CLD\_ROCC during the last ~18,000 years (0.37) (Supplementary Table 2). A closer look into the multi-millennial intervals (Supplementary Tables 3–7) reveals a range of significant correlations from moderate positive (~18–14 ka: 0.48) to strong positive (~14–12 ka: 0.72), weak negative (~12–8 ka: −0.15), and non-significant (~8–4 ka).

### 3.2. Isla Grande de Chiloé

Five sites from Isla Grande de Chiloé, spread along a ~80 km north-south transect through the central and southern portions of the island, show approximately half the raw macroscopic CHAR values observed in records from the Chilean Lake District (Fig. 1, Supplementary Table 1). The Isla Grande de Chiloé sites are located near the western coast (L. Quilque), eastern foothills of the central Coastal Range (L. Tarumán), eastern coast (L. Lepué, L. Oqueldán), and the southern coast (L. Huillin). The macroscopic charcoal records from sites located in Isla Grande de Chiloé (IGC\_CHACC) (Supplementary Fig. 3) produce a compilation curve (Fig. 5) that reveals significant negative values between ~18–17.6 ka and ~16.1–14.1, interrupted by a rise between ~17.6–16.1 ka that peaked between ~17.4–17.1 ka and at ~16.3 ka. Low values prevail between

~14.1–11 ka, followed by a rapid rise that leads to permanent positive anomalies between ~10.8–9.1 ka with significant maxima at ~10.5 ka and between ~9.7–9.3 ka. A sudden decline leads to values below the mean between ~9–5 ka terminated by a rise that culminated in a peak above the mean at ~4.4 ka and declined rapidly back into negative anomalies. A steady rise at ~3.3 ka led to significant high values between ~2.4–0.8 ka and ~0.5–0.1 ka, separated by a conspicuous reversal. Period-wise Kruskal ANOVAs on the multi-millennial intervals (Supplementary Fig. 2) reveal that: ~4–0 ka > ~12–8 ka = ~8–4 ka > ~14–12 ka > ~18–14 ka.

The LOI<sub>925</sub> and MS data show a ubiquitous thick and coarse tephra in all Isla Grande de Chiloé sites at ~11 ka, along with a thin tephra dated at ~8.2 ka (Supplementary Fig. 3). Some sites record a ~6.3 ka (L. Quilque, L. Oqueldán) and a ~2.3 ka-old tephra (L. Tarumán, L. Lepué). The MS data from L. Huillin show the ~11 ka tephra but fails to detect the ~8.2 ka horizon, evident in the LOI data (not shown).

The ROC compilation curve for the Isla Grande de Chiloé sites (IGC\_ROCC) (Fig. 5) shows predominance of positive anomalies between ~17.7–13.8 ka with significant high values between ~17.4–16.9 ka, the highest of the entire record, and ~14.7–14.4 ka. An interval with large-magnitude oscillations around the mean follows between ~13.8–7.7 ka, with significant positive values

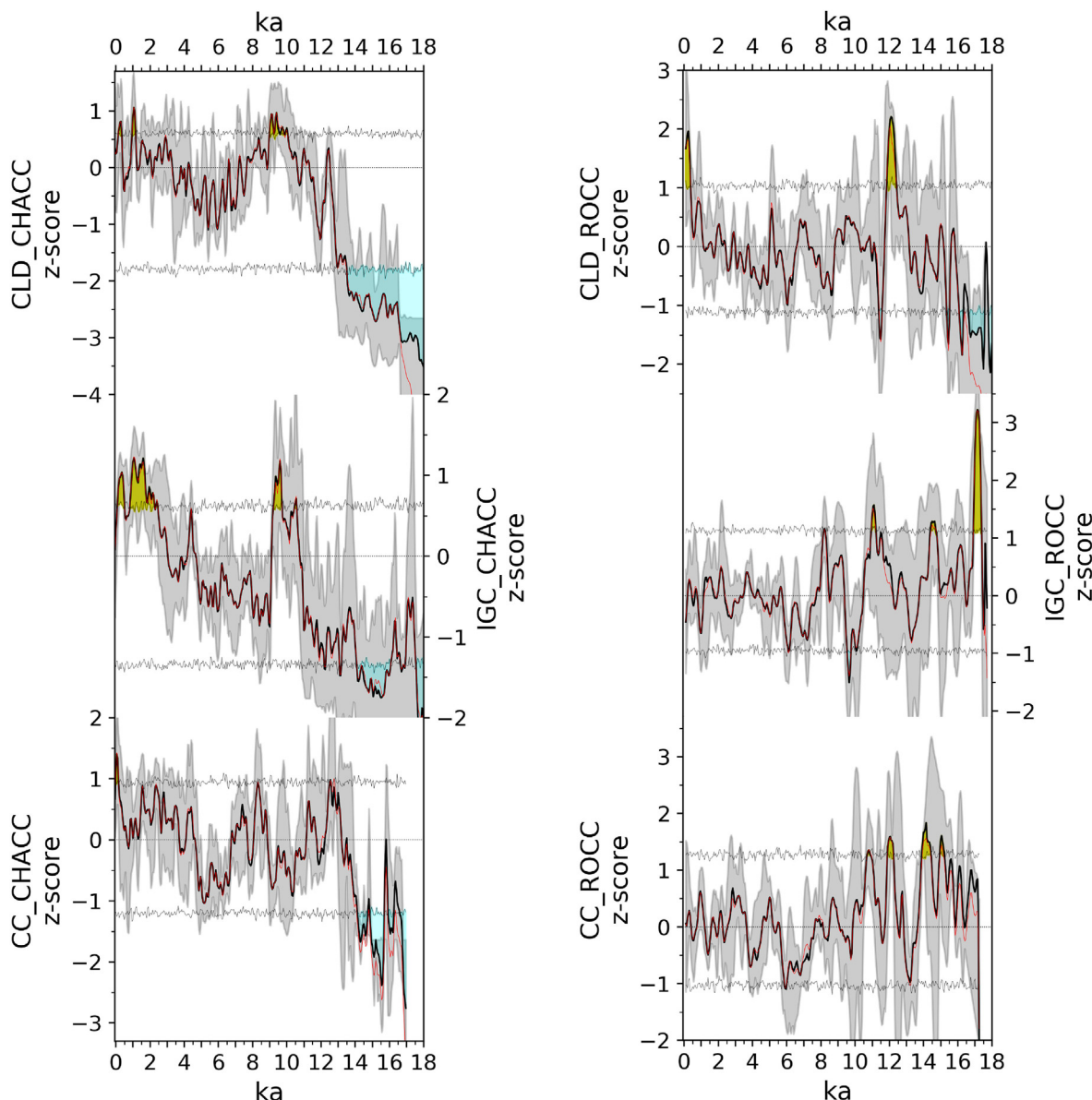


**Fig. 5.** Macroscopic charcoal and Rates-of-Change compilation curves from the Chilean Lake District (CLD), Isla Grande de Chiloé (IGC), and Chiloé Continental (CC). The black solid lines show a robust LOWESS fit applied to each compilation, embedded within a gray shading that portrays the result of 1000 bootstrap iterations. The horizontal lines mark the mean of the last ~12,000 years (straight line) and the 95% confidence intervals as determined by a circular block bootstrap with 1000 iterations. The yellow/cyan shading show values above/below the 97.5th/2.5th bootstrapped percentiles, respectively. The red line corresponds to the mean of the bootstrapped values. (For interpretation of the references to colour in this figure legend, the reader is referred to the Web version of this article.)

between ~11.2–11 ka, a prominent peak between ~8.3–8.1 ka, and significant low values between ~9.8–9.6 ka. A subsequent decline leads to predominance of negative anomalies between ~7.7–5.8 ka, and low-magnitude oscillations around the mean between ~5.8 ka and the present. The magnitude of the compiled ROC values along the multi-millennial intervals (Supplementary Fig. 2) ranks in the following order: ~18–14 ka > ~12–8 ka > ~14–12 ka = ~4–0 ka > ~8–4 ka.

The IGC\_CHACC shows a weak negative correlation with IGC\_ROCC (−0.36) over the last ~18,000 years (Supplementary Table 2). When partitioning the IGC\_ROCC dataset in multi-millennial intervals (Supplementary Tables 3–7) this relationship ranges from strong negative (~12–8 ka: −0.69) to moderate positive (~8–4 ka: 0.4), with non-significant correlations in the remaining intervals.

The IGC\_CHACC shows a strong positive correlation with CLD\_CHACC (0.77) over the last ~18,000 years (Supplementary Table 2), which varies from non-significant (~18–14 ka), weak negative (~14–12 ka: −0.39), weak positive (~8–4 ka: 0.24), and moderate positive (~12–8 ka: 0.6, ~4–0 ka: 0.55) (Supplementary Tables 3–7). The IGC\_ROCC shows a weak negative correlation with CLD\_ROCC (−0.23) over the last ~18,000 years, which ranges from weak negative (~18–14 ka: 0.23, ~12–8 ka: −0.36) to non-significant.

### 3.3. Chiloé Continental

The Chiloé Continental region is constrained by five sites (Fig. 1, Supplementary Table 1), two of which are located near the eastern Seno Reloncaví coast (Puelche section, L. Proschle) (Moreno, 2020),

one site in the core of the northern Patagonian Andes just east of the continental divide (L. Espejo) (Jara et al., 2019), a site near the Chaitén coast (L. Teo) (Henríquez et al., 2015), and a site in the core of the Andes just west of the continental divide (L. Negro) (Moreno et al., 2021b) in southern Chiloé Continental. The charcoal records exhibit ample differences in their stratigraphy and magnitudes (Supplementary Fig. 4), attesting to significant north-south and east-west environmental heterogeneities along this broad mountainous region. One important feature of this sector of the Andes is the presence of multiple eruptive centers that have been active over the last ~18,000 years, with differences in the timing, recurrence, and magnitude of explosive events among sectors.

The macroscopic charcoal compilation curve from Chiloé Continental (CC\_CHACC) (Fig. 5) shows predominance of significant negative anomalies between ~17–14.1 ka, with short-lived increases that culminated in peaks at ~16.4 ka, ~15.8 ka, and ~14.8 ka. A sustained rise starts at ~14.3 ka and culminates in significant high values at ~12.5 ka, followed by a decline into negative values until ~11.9 ka and a subsequent increase that peaks at ~11.3 ka. A decline then leads to persistent negative values between ~11.1–8.9 ka, predominance of positive values between ~8.9–6.8 ka with a prominent maximum at ~8.3 ka, and a brief reversal into negative values between ~8.1–7.7 ka. A subsequent decline leads to persistent negative values between ~6.7–4.7 ka terminated by a sustained rise that leads to predominance of positive values between ~4.7 ka and the present, within which we observe significant high values between ~0.2 ka and the present. We detect significant differences between intervals (Supplementary Fig. 2), with ~4–0 ka > ~14–12 ka > ~12–8 ka > ~8–4 ka > ~18–14 ka.

We detect 29 siliciclastic peaks since ~17.3 ka that correspond to visible tephra and cryptotephra layers in L. Proschle (Supplementary Fig. 4). The Puelche Section includes 16 tephra layers since ~16.3 ka and a systematic increase in siliciclastic density from ~4 ka to the present as a result of slumping from the surrounding diamicton-dominated slopes. The L. Espejo record contains 28 tephra layers since ~15.5 ka, L. Teo features 26 tephra since ~9.8 ka, and L. Negro has 27 tephra layers since ~12.7 ka.

The ROC records from sites located in Chiloé Continental (Supplementary Fig. 4) constitute the basis for a compilation curve (CC\_ROCC) (Fig. 5) that shows predominance of positive anomalies between ~17.2–13.7 ka, and significant high values between ~15.2–15 ka and ~14.4–13.9 ka. A steady decline led to strong negative anomalies at ~13.2 ka, after which we observe large-magnitude millennial-scale oscillations between ~13.2–9.8 ka with significant high values between ~12.2–11.9 ka and ~10.9–10.8 ka. From ~10.7 ka to the present we observe oscillations of damped magnitude at millennial timescale, featuring a trough with significant low values at ~5.9 ka. The Kruskal ANOVAs reveal (Supplementary Fig. 2): ~18–14 ka > ~14–12 ka = ~12–8 ka > ~4–0 ka > ~8–4 ka.

The correlations between CC\_CHACC with CLD\_CHACC and IGC\_CHACC (Supplementary Table 2) are strong (0.69) and moderate (0.52) over the last ~18,000 years, respectively. The relationships change when analyzing the multi-millennial intervals (Supplementary Tables 3–7): the correlations between CC\_CHACC and CLD\_CHACC range from strong positive (~14–12 ka: 0.66) to weak positive (~18–14 ka: 0.39, ~4–0 ka: 0.35, ~8–4 ka: 0.31) and weak negative (~12–8 ka: -0.19), while CC\_CHACC and IGC\_CHACC range from weak positive (~18–14 ka: 0.4, ~8–4 ka: 0.39) to weak negative (~14–12 ka: -0.33), moderate negative (~12–8 ka: -0.57), and non-significant (~4–0 ka).

The correlation between CC\_ROCC with CLD\_ROCC and IGC\_ROCC are non-significant and moderate (0.46) over the last ~18,000 years, respectively (Supplementary Table 2). The relationships change when analyzing the multi-millennial intervals

(Supplementary Tables 3–7): the correlations between CC\_ROCC and CLD\_ROCC are mainly non-significant except for a weak positive interval (~18–14 ka: 0.37), while CC\_ROCC and IGC\_ROCC range from strong positive (~14–12 ka: 0.67) to moderate positive (~8–4: 0.51), weak positive (~12–8 ka: 0.33), moderate negative (~4–0 ka: -0.48), and non-significant (~18–14 ka).

### 3.4. Regional, Andean, Western Upwind Environments, and sub-continental compilations

The macroscopic charcoal compilation curve for all NWP sites reported in this study (NWP\_CHACC) (Fig. 6) shows significant low values between ~18–13.1 ka with a modest rise between ~17.1–15.8 ka, followed by a gradual increase that starts at ~14.1 ka and stabilizes between ~13.5–13.1 ka. A sharp increase begins at ~13.1 ka and culminates in a positive anomaly peak at ~12.5 ka, followed by a steady decline into negative values until ~11.9 ka. An increase leads to values around the mean between ~11.3–8.1 ka, within which we observe significant high values between ~10–9.4 ka and at ~8.3 ka. A shift toward negative anomalies prevails between ~8.1–3.6 ka with a conspicuous minimum between ~6–4.8 ka, and a sustained rise that starts at ~4.8 ka leading to a prominent positive anomaly peak at ~4.4 ka. An increase leads to the predominance of significant high values between ~3.1 ka and the present, with maxima at ~1.6 ka, ~1.1 ka, and ~0.3 ka, separated by prominent declines. The Kruskal ANOVA (Supplementary Fig. 5) detects significant differences within and among all T1 and Holocene intervals, with ~4–0 ka > ~12–8 ka > ~8–4 ka > ~14–12 ka > ~18–14 ka.

The ROC compilation curve for all NWP sites (NWP\_ROCC) (Fig. 6) shows predominance of negative anomalies and significant low values between ~18–17.3 ka, along with discrete positive anomalies between ~17.3–13.8 ka with significant high values between ~17.2–17 ka, and a decline that leads to persistent negative anomalies between ~13.8–13.1 ka with significant low values at ~13.3 ka. The interval between ~13.1–10.4 ka features large-magnitude oscillations with a predominance of positive anomalies and significant high values between ~12.3–11.9 ka and ~11.2–10.9 ka. From ~10.4 ka to the present we observe a decline in the magnitude of oscillations at millennial timescale, with modest values around the mean. Among these we emphasize significant low values between ~6.3–5.9 ka and significant high values at ~0.3 ka. The Kruskal ANOVA detects significant differences in most intervals (Supplementary Fig. 5), with ~18–14 ka > ~14–12 ka = (~12–8 ka > ~4–0 ka) > ~8–4 ka.

We detect a weak negative correlation between NWP\_CHACC and NWP\_ROCC over the last ~18,000 years (-0.17) (Supplementary Table 2). The breakdown of this relationship at multi-millennial scale (Supplementary Tables 3–7) shows a range from moderate positive correlations (~4–0 ka: 0.53; ~14–12 ka: 0.43) to strong negative (~12–8 ka: -0.61) and non-significant (~18–14 ka; ~4–0 ka) correlations.

We combined the data from the Chilean Lake District sites located closest to the Andean foothills (L. Pichilafquén, L. Fonk, L. Reflejos) and all sites from Chiloé Continental to generate the Andean macroscopic Charcoal Compilation Curve (AND\_CHACC), and a Rates-of-Change compilation curve for Andean sites (AND\_ROCC) from NWP (Fig. 6). This cluster allows comparisons with other sites located >35 km west of the Andes, which are separated from active eruptive centers by large water bodies (Lago Llanquihue, Seno Reloncaví, and the Chilotan Sea). This distinction explicitly acknowledges the westward decline in the frequency and thickness of tephra layers, and the natural firebreaks established by large lakes and seaways. The cluster distal to the Andes includes all sites from Isla Grande de Chiloé in addition to L. Pichilaguna and L. El Salto

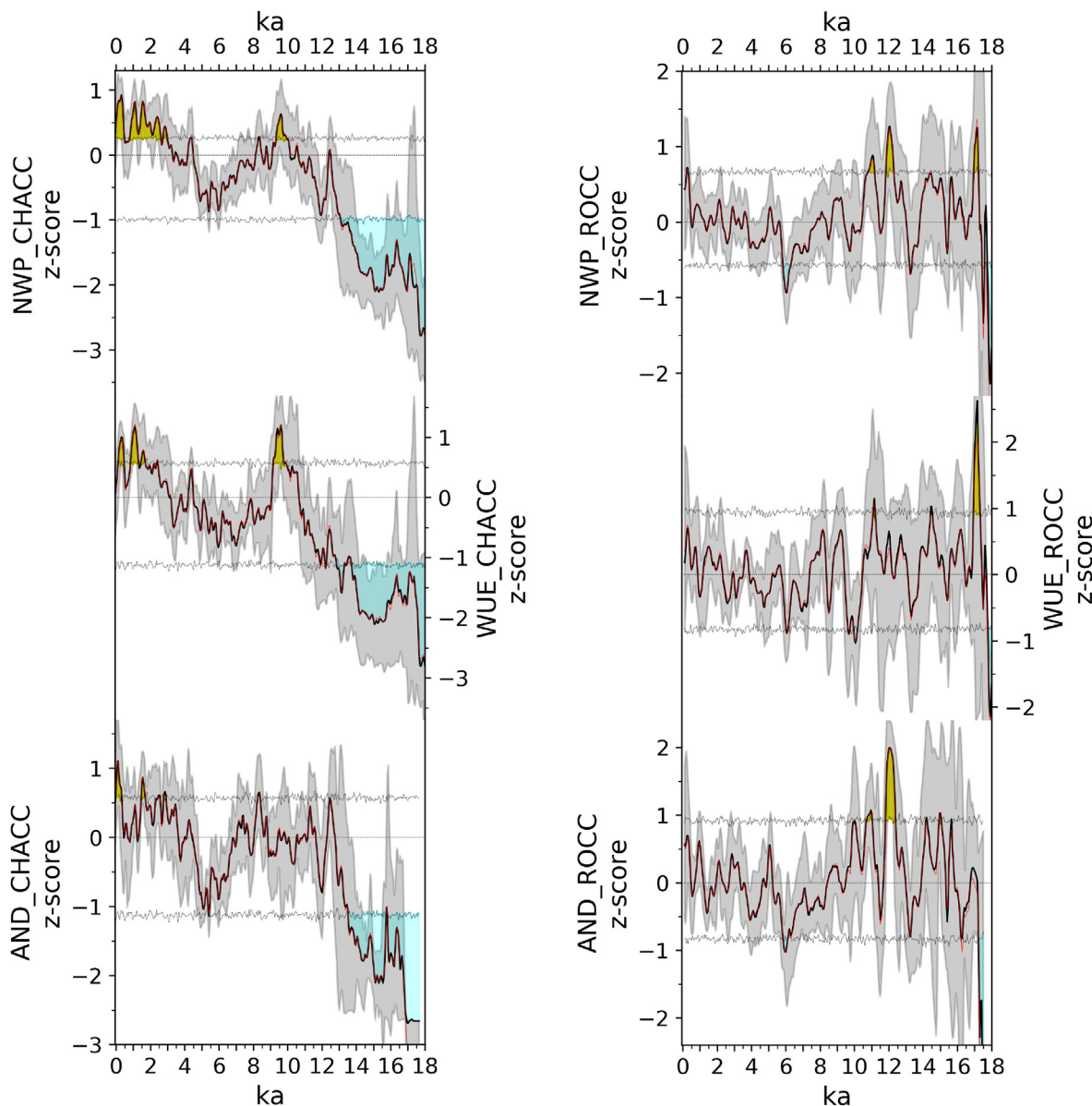


**Fig. 6.** Compiled macroscopic charcoal and Rates-of-Change curves at regional scale (Northwestern Patagonia = NWP) and proximity to the Andes: Andean (AND) and Western Upwind Environments (WUE).

from the Chilean Lake District. Data from this cluster define the Western Upwind Environments Charcoal Compilation Curve (WUE\_CHACC), and the Western Upwind Environments Rates-of-Change Compilation Curve (WUE\_ROCC) from NWP.

The NWP\_CHACC shows very strong correlations with the AND\_CHACC and WUE\_CHACC (both  $r = 0.95$ ) over the last ~18,000 years (Supplementary Table 2), which breakdown in the following manner (Supplementary Tables 3–7): correlations between NWP\_CHACC and AND\_CHACC are all positive and range from very strong (~14–12 ka: 0.95, ~8–4 ka: 0.88, ~18–14 ka: 0.8) to strong (~4–0: 0.71) and moderate (~12–8 ka: 0.48), while NWP\_CHACC and WUE\_CHACC also correlate positively and range from very strong (~4–0 ka: 0.9, ~12–8 ka: 0.86, ~14–12 ka: 0.82) to strong (~18–14 ka: 0.74) and moderate (~8–4 ka: 0.64). We observe offsets in the timing and magnitude of events and significant positive anomalies (Fig. 6). These differences are maximized when comparing the AND\_CHACC and WUE\_CHACC datasets ( $r: 0.8$ ) (Supplementary Table 2), which show:

- Significant high AND\_CHACC values occur at ~12.5 ka, ~8.3 ka, ~2.8 ka, ~2.5 ka, between ~1.7–1.5 ka and ~0.3–0 ka, whereas significant high WUE\_CHACC values occur between ~9.8–9.2 ka, at ~2.4 ka, and between ~1.7–1.5 ka, ~1.3–0.9 ka, and ~0.5–0.2 ka.
- AND\_CHACC values are higher between ~13.3–10.7 ka, ~8.9–6.6 ka, and ~3.6–2.8 ka. WUE\_CHACC values, on the other hand, are higher between ~10.7–9 ka, at ~4.4 ka, and between ~1.4–0.7 ka.
- The magnitudes in AND\_CHACC are ~4–0 ka > ~12–8 ka > ~8–4 ka = ~14–12 ka > ~18–14 ka (Supplementary Fig. 5).
- The magnitudes in the WUE\_CHACC are ~4–0 ka > ~12–8 ka > ~8–4 ka > ~14–12 ka > ~18–14 ka.

The NWP\_ROCC shows very strong (0.82) and strong (0.73) correlations with the AND\_ROCC and WUE\_ROCC datasets (Supplementary Table 2), respectively, which breakdown in the following manner (Supplementary Tables 3–7): correlations

between NWP\_ROCC and AND\_ROCC are all positive and range from very strong (~14–12 ka: 0.95, ~8–4 ka: 0.81, ~4–0 ka: 0.8) to strong (~18–14 ka: 0.72) and moderate (~12–8: 0.64), while NWP\_ROCC and WUE\_ROCC also correlate positively and range from strong (~8–4 ka: 0.76, ~18–14 ka: 0.75, ~14–12 ka: 0.73, ~12–8 ka: 0.72) to moderate (~4–0 ka: 0.61). We observe offsets in the timing and magnitude of events and significant positive anomalies (Fig. 6). The differences are highest between AND\_ROCC and WUE\_ROCC datasets ( $r: 0.23$ ) (Supplementary Table 2), namely:

- The largest positive anomalies in WUE\_ROCC occur between ~17.4–16.9 ka at times of predominant negative anomalies in AND\_ROCC. Conversely, the largest positive anomalies in AND\_ROCC occur between ~12.4–11.8 ka at times of modest positive anomalies in WUE\_ROCC.
- WUE\_ROCC declines to persistent negative anomalies between ~10.5–9.4 ka, the lowest and most persistent of the Holocene record, whereas AND\_ROCC shifts in the opposite direction.
- The magnitudes in WUE\_ROCC are ~18–14 ka > ~14–12 ka = ~12–8 ka = ~4–0 ka > ~8–4 ka (Supplementary Fig. 5).
- The magnitudes in AND\_ROCC are ~18–14 ka = ~14–12 ka = ~12–8 ka > ~4–0 ka > ~8–4 ka.

We developed a Temperate South American Charcoal Compilation (TSA\_CHACC) for sites  $>40^{\circ}\text{S}$  constrained by at least five radiocarbon dates using data from 19 sites downloaded from the Global Paleofire Database (Fig. 7). This compilation is essentially

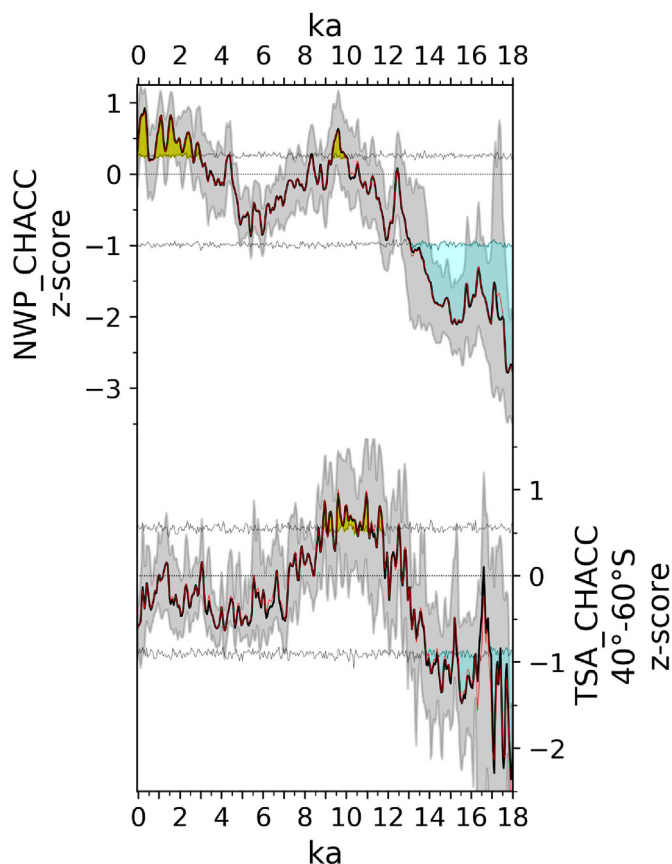


**Fig. 7.** Comparison of the regional compilation of Northwestern Patagonia macroscopic charcoal sites (NWP\_CHACC) and the Temperate South America Charcoal Compilation Curve (TSA\_CHACC) based on data downloaded from the Global Paleofire Database.

identical to the original curve published by Power et al. (2008) for southern South America, and our updated synthesis including all South American sites  $>30^{\circ}\text{S}$  included in the Global Paleofire Database ( $r: 0.99$ ) (not shown in this paper). We observe persistently negative anomalies between ~18–12.9 ka, except for a positive peak at ~16.6 ka, with predominance of significant low values between ~18–13.8 ka. A transitional phase occurs between ~12.9–12 ka, followed by predominance of positive anomalies between ~12–7.2 ka. Significant high values occur at ~12.6 ka and multiple times between ~11.8–8.9 ka. Negative anomalies prevail from ~7.2 ka onward, overprinted by modest positive peaks centered at ~6.7 ka, ~3.1 ka, and ~1.3 ka. A period-wise Kruskal ANOVA on the TSA\_CHACC series (Supplementary Fig. 6) reveals that ~12–8 ka > ~14–12 ka = (~4–0 ka > 12–8 ka) > ~18–14 ka.

The Holocene NWP\_CHACC diverges from the TSA\_CHACC starting with a rise that started at ~4.6 ka and peaked at ~4.3 ka, along with the predominance of significant high values from ~3.3 ka to the present. The NWP\_CHACC and TSA\_CHACC show a strong correlation over the last ~18,000 years (0.65) (Supplementary Table 2), in particular very strong between ~14–12 ka (0.89) along with weak correlations between ~8–4 ka (0.28) and ~4–0 ka (0.39), along with non-significant during the remaining intervals (Supplementary Tables 3–7).

### 3.5. Radiocarbon-dated archaeological sites

Our synthesis of radiocarbon-dated archaeological sites between latitudes  $40^{\circ}\text{S}$  and  $46^{\circ}\text{S}$  (Fig. 8, Supplementary Fig. 7, Supplementary Table 8) includes a total of 294 ages spanning the last ~19,300 years. Seventy-eight (26.5%) of them were excluded from the analysis because they were either unfit (e.g., high-sigma, too recent), lacked critical data, or were not indicative of an anthropogenic origin (i.e., association with the archaeological context). Summed probability distributions (SPD) show a conspicuous geographic structure which we discuss focusing on the portion of the record spanning the last ~18,000 years.

#### 3.5.1. Chilean Lake District

Three sites located in the southern portion of the Chilean Lake District (Supplementary Fig. 7) include dates that span the interval between ~19.3–13.2 ka (Supplementary Table 8) and they all occur within an area  $<5$  ha in the locality of Monte Verde. The earliest ages correspond to Monte Verde I, with a large range (~19.3–13.8 ka) that overlaps with the overlying horizon Monte Verde II and Chinchihuapi 1, constrained between ~14.6–13.9 ka (Supplementary Table 8). The Pilauco site, located in the northern portion of the Chilean Lake District, affords ages between ~15.9–13.2 ka (Pino and Astorga, 2020). Only two radiocarbon dates from sites from the Longitudinal Valley span the interval between ~12.5–10.2 ka (Dillehay et al., 2019): the younger age of Chinchihuapi 1 and that from the Río Bueno site (Supplementary Table 8). These are separated by a ~4000-year long gap from the bulk of radiocarbon-dated sites located along the southern and northernmost coasts of the Chilean Lake District.

The SPD for archaeological sites located in the Chilean Lake District (CLD\_SPD) (Fig. 8) shows absence of radiocarbon dates between ~18–16 ka, a variable cluster of ages between ~16–13.2 ka with peaks at ~15.8 ka and ~13.8 ka, followed by a decline with intermittent low-magnitude increases that peaked at ~12.3 ka and ~10.5 ka. The interval ~10.5–6.5 ka shows absence of radiocarbon dates that give way to a millennial-scale alternation of intermediate and low SPD values approaching zero between ~6.4–3.8 ka. A more permanent signal with intermediate values is evident between ~3.4–2 ka, followed by a distinct gap between ~2–0.8 ka within which we observe a brief low-magnitude peak between ~1.5–1.2

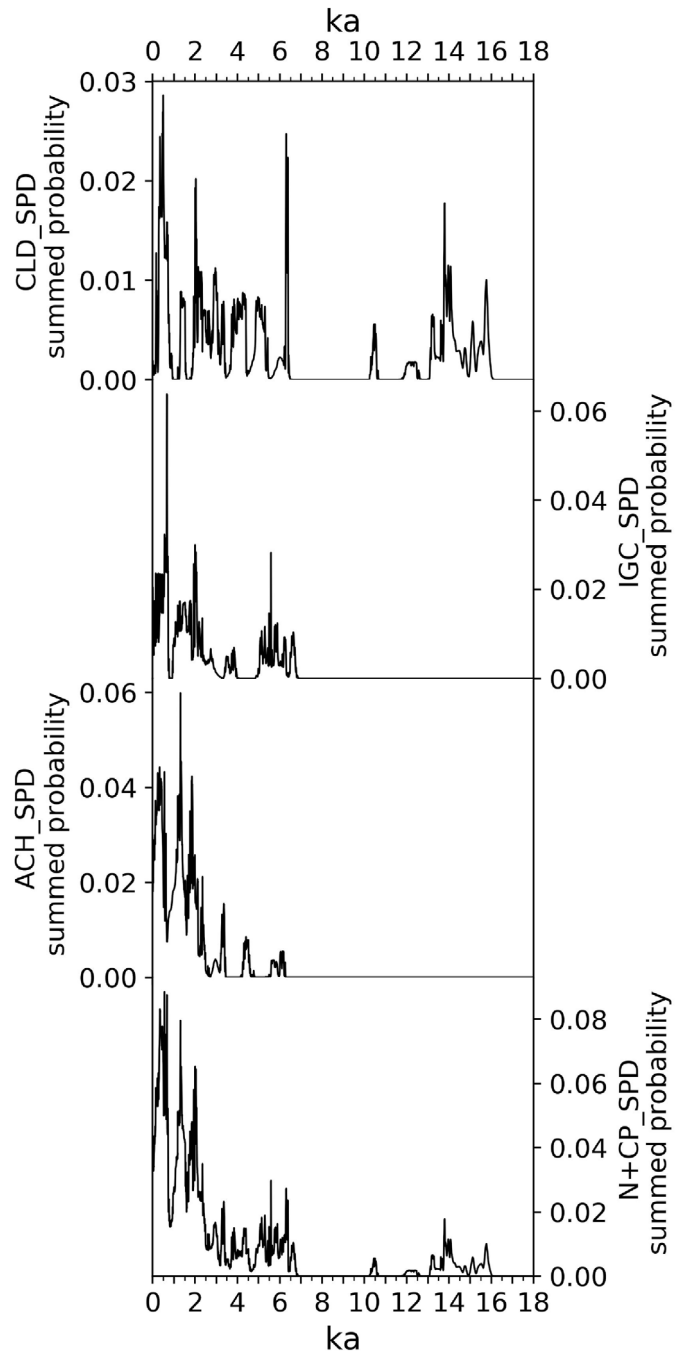


**Fig. 8.** Summed Probability Distribution (SPD) of radiocarbon-dated archaeological sites for the different geographic units considered in this study, along with a regional synthesis.

ka. The CLD\_SPD then increases between ~0.8–0.3 ka, achieving the largest peak on record that declines abruptly toward the present.

Period-wise Kruskal ANOVAs applied to the CLD\_SPD dataset ([Supplementary Fig. 8](#)) reveal significant differences within and among all T1 and Holocene intervals. The analysis shows that: ~4–0 ka > ~14–12 ka > ~8–4 ka > ~18–14 ka > ~12–8 ka.

### 3.5.2. Isla Grande de Chiloé

We included dates from a cluster of caves located within Punta Vilcún ([Supplementary Fig. 7, Supplementary Table 8](#)), a prominent bedrock knob near Chaitén in Chiloé Continental ([Labarca et al., 2021](#),

2021), as part of Isla Grande de Chiloé because: (a) they are located near the coast of the Chiloé Interior Sea, within the latitudinal range of Isla Grande de Chiloé, (b) these sites are concentrated in narrow geographic and temporal contexts and, thus, (c) are not very informative about the Chiloé Continental region to merit a separate analysis. Radiocarbon-dated archaeological sites in Isla Grande de Chiloé span the last ~6700 years with an initial intermittence that leads to a more permanent presence over the last ~4000 years, and a maximum during the last millennium ([Fig. 8, Supplementary Table 8](#)).

The SPD from sites located in Isla Grande de Chiloé (IGC\_SPD) ([Fig. 8](#)) features a distinct cluster of dates between ~6.7–5 ka, showing an alternation between multi-century increases that reach intermediate magnitudes and declines that approach zero. Low IGC\_SPD values occur between ~5–3 ka, interrupted by a brief increase between ~4–3.5 ka, followed by a gradual rise that culminates with a prominent peak at ~2 ka and persistence of high SPD values until ~1 ka. A decline leads to a conspicuous interval with zero values between ~1–0.8 ka that gives way to an abrupt increase that culminates in the largest-magnitude peak of the entire record between ~0.8–0.5 ka, followed by a gradual decline toward the present. The period-wise Kruskal ANOVAs applied to the IGC\_SPD dataset ([Supplementary Fig. 8](#)) allows the following distinctions: ~4–0 ka > ~8–4 ka. The IGC\_SPD and CLD\_SPD series show moderate correlation during the last ~18,000 years (0.49) ([Supplementary Table 2](#)).

### 3.5.3. Archipiélago de los Chonos

The inventory of radiocarbon-dated archaeological sites from Archipiélago de los Chonos is based on a research program intended to measure the temporal distribution of human activity across the archipelago, and thus considered radiocarbon dating all available archaeological evidence minimizing biases in the construction of chronology ([Reyes et al., 2019a](#)). The record shows intermittent human occupations between ~6.3–2.5 ka that shift to a more permanent presence thereafter, and the highest frequency of sites over the last ~2000 years. The SPD from sites located in Archipiélago de los Chonos (ACH\_SPD) ([Fig. 8](#)) shows values approaching zero between ~6.3–2.5 ka with a distinct clustering of dates that produce low-magnitude values between ~6.3–5.5 ka, ~4.6–4.2 ka, ~3.2–2.8 ka, and an increase of intermediate magnitude between ~3.4–3.2 ka. A steady increase starts at ~2.5 ka and culminates in a prominent peak at ~1.8 ka, followed by a brief reversal and a subsequent increase that peaked at ~1.3 ka, the largest in the entire record. A conspicuous decline ensued until it reaches its minimum at ~0.7 ka, succeeded by a rapid rise that peaked at ~0.3 ka, followed by a decline toward the present. We find significant differences between the Holocene intervals in the ACH\_SPD dataset, with ~4–0 ka > ~8–4 ka ([Supplementary Fig. 8](#)). The ACH\_SPD series shows weak (0.38) and strong (0.74) correlations with CLD\_SPD and IGC\_SPD over the last ~18,000 years, respectively.

### 3.5.4. Regional compilation of radiocarbon-dated archaeological sites

A compilation of all radiocarbon dates from archaeological sites located in Northwestern and coastal Central Western Patagonia (N+CP\_SPD) ([Fig. 8](#)) reveals persistently low values between ~16–10.5 ka with modest peaks at ~15.8 ka and ~14 ka, that shift to intermittent occurrences between ~13.2–10.5 ka and give way to a gap in radiocarbon dates that persists until ~6.8 ka. An interval of fluctuating but continuous low-magnitude SPD values prevails between ~6.8–2.5 ka, followed by a rapid increase that leads to successively higher peaks at ~2 ka, ~1.2 ka, and ~0.5 ka. These peaks are separated by distinct declines, the largest of which takes place between ~1.2–0.8 ka. The N+CP\_SPD values then plummet toward

the present after ~0.3 ka.

We find statistically significant differences within and among all T1 and Holocene N+CP\_SPD intervals ([Supplementary Fig. 8](#)). Our analyses reveal that: ~4–0 ka > ~8–4 ka > ~14–12 ka > ~18–14 ka > ~12–8 ka. Significant correlations between N+CP\_SPD and charcoal compilations spanning the last ~18,000 years include (in decreasing order of magnitude): IGC\_CHACC (0.57), WUE\_CHACC (0.46), NWP\_CHACC (0.42), AND\_CHACC (0.33), and CC\_CHACC (0.29) ([Supplementary Table 2](#)). The scarcity of radiocarbon dates and intermittence of SPDs through the ~14–12 ka and ~12–8 ka intervals preclude any meaningful statistical analyses and conclusions, but they are significant in supporting the concept of a negligible contribution of humans as triggers for wildfires through those intervals. The correlations during the ~8–4 ka interval become weak negative (NWP\_CHACC: 0.26), moderate negative (CC\_CHACC: -0.46, AND\_CHACC: -0.49), or non-significant. The relationship changed again during the ~4–0 ka interval becoming strong (IGC\_CHACC: 0.66) or moderate positive (WUE\_CHACC: 0.56, NWP\_CHACC: 0.51), depending on the geographic scale of analysis ([Supplementary Tables 3–7](#)).

The correlations between N+CP\_SPD and ROC compilations spanning the last ~18,000 years are weak positive (IGC\_ROCC: 0.09; WUE\_ROCC: 0.09) or weak negative correlation (CC\_ROCC: -0.16) ([Supplementary Table 2](#)). Between ~8–4 ka the only significative correlation is with CLD\_ROCC (-0.25). The relationship between N+CP\_SPD and ROC compilations changes during the ~4–0 ka interval toward moderate positive at multiple spatial scales (CLD\_ROCC: 0.55, WUE\_ROCC: 0.5, NWP\_ROCC: 0.42) and weak negative (CC\_ROCC: -0.25) ([Supplementary Tables 3–7](#)).

## 4. Discussion

### 4.1. Spatial and temporal CHAR patterns

The macroscopic charcoal data presented in this study suggest that wildfires have been ubiquitous throughout NWP since ~18 ka, with important variations in their temporal and geographic structure. Comparability and compatibility among the charcoal records analyzed in this study are maximized by considering records retrieved from carefully selected small closed-basin lakes, located in similar geomorphologic settings, using the same sampling and processing protocols, independently constrained by precise radiocarbon chronologies (total: 212 dates, mean: 14 AMS dates/site [min: 6, max: 23], mean: 1333 years/<sup>14</sup>C AMS date per site [min: 431, max: 2859]), and using the same analytical approach and quantification units. Consequently, the data are strongly consistent and enable direct comparisons among sites using the macroscopic charcoal accumulation rate (CHAR) parameter.

Fires in NWP over the last ~18,000 years have taken place in the context of grassland/scrubland, woodland, and broad-leaved evergreen temperate rainforest vegetation ([Henríquez et al., 2015](#); [Jara and Moreno, 2014](#); [Jara et al., 2019](#); [Moreno, 2020](#); [Moreno et al., 2018a, 2022](#); [Pesce and Moreno, 2014](#)), hydroclimate changes at millennial and centennial timescales ([Henríquez et al., 2021b](#); [Moreno and Videla, 2016](#)), explosive volcanic activity ([Alloway et al., 2017a,b](#); [Bertrand et al., 2008](#); [Naranjo et al., 2017](#); [Naranjo and Stern, 2004](#); [Singer et al., 2008](#)), and human presence in the region ([Campbell and Quiroz, 2015](#); [Dillehay, 1989](#); [Dillehay et al., 2015](#); [Méndez, 2013](#); [Reyes, 2020](#)).

Raw macroscopic CHAR values are highest in the northern sites (Chilean Lake District: L. Pichilafquén, L. Fonk), decline southward, and reach conspicuous minima in western coastal (Isla Grande de Chiloé: L. Quilque, L. Huillin; Chiloé Continental: L. Proschle, L. Teo) and high elevation sites in the core of northern Chiloé Continental (L. Reflejos) ([Supplementary Figs. 1, 3, 4](#)). This geographic

distribution of CHAR values mirrors the modern north-to-south and low-to-high elevation increase in annual precipitation and decrease in precipitation seasonality in NWP ([Fig. 3](#)). Raw CHAR over the last ~18,000 years is significantly highest in the Chilean Lake District, intermediate in Chiloé Continental, and lowest in Isla Grande de Chiloé ([Supplementary Fig. 8](#)). In addition, the northernmost sites are located near the Andean foothills where the number of tephra layers is maximal ([Bertrand et al., 2008](#); [Singer et al., 2008](#); [Henríquez et al., 2021a, 2021b](#); [Jara and Moreno, 2014](#); [Moreno et al., 2021b](#); [Naranjo et al., 2017](#); [Alloway et al., 2022](#)). The Redundancy Analysis ordination shows that the explanatory variables annual and seasonal temperature and precipitation gradients account for 37.9% of the total variance along RDA Axis 1, and explosive volcanism account for 25.3% of the variance along RDA Axis 2. The covariation between the distance to the nearest eruptive center and mean spacing between clastic peaks along RDA Axis 2 suggests that tephra fallout is maximal in the vicinity of active volcanic centers. Together, RDA Axes 1 and 2 account for 63.2% of the total variance of the explanatory environmental variables. When linearly regressed upon this ordination, Macroscopic CHAR shows a highest magnitude factor loading of -0.72 along RDA Axis 1, implying that gradients in annual and seasonal precipitation and temperature are the main explanatory variables for the mean CHAR magnitude over the last ~1000 years, while seasonality and geographical location with respect to coasts and eruptive centers play a secondary or even orthogonal role.

Tephra layers are ubiquitous throughout the region since ~18 ka, with a distinct minimum in Isla Grande de Chiloé (2–3 tephra) and the lowlands of the Chilean Lake District (3–4 tephra: L. Pichilaguna and L. El Salto) ([Supplementary Figs. 1, 3, 4](#)). The number increases toward the western Andean foothills in the northern (25–30 tephra) and southern portions of the Chilean Lake District (18 tephra). The central portion of Chiloé Continental features the highest abundance of tephra layers upon its western coast (26 tephra since ~10 ka: L. Teo) and in the core of northern Chiloé Continental (28 tephra since ~16 ka: L. Espejo). The southern core of Chiloé Continental features 27 tephra layers since ~12.7 ka (L. Negro). This eastward increase in the number and thickness of tephra layers reaches maxima in the vicinity of active eruptive centers (Volcán Puyehue-Cordón Caulle complex, V. Osorno-V. Calbuco, V. Chaitén-V. Michimahuida, and V. Melimoyu) ([Figure 1](#)). This relationship is evident in the ordination along the RDA Axis 2.

We posit that heightened precipitation seasonality and frequent volcanic disturbance have enhanced fire activity (raw macroscopic CHAR values) in the northern sector not only during the last ~1000 years but since the end of the LGM ([Fig. 3](#)). Conversely, attenuated precipitation seasonality and lower recurrence of explosive volcanic events may have inhibited the occurrence of fires in the southern coastal sectors ([Henríquez et al., 2015](#); [Moreno et al., 2021b](#)). The mountainous region of Chiloé Continental represents an intermediate condition given its southern location along the gradient in annual precipitation and rainfall seasonality, and the proximity to active volcanic centers ([Henríquez et al., 2015](#); [Jara and Moreno, 2014](#); [Moreno et al., 2021b](#)).

The compiled NWP macroscopic charcoal curve (NWP\_CHACC) shows that fire activity was significantly low between ~18–13.1 ka ([Fig. 5](#)). Variability at smaller spatial scale prior to ~13.1 ka includes increases that peak between ~17.4–17.1 ka and at ~16.3 ka in Isla Grande de Chiloé, along with prominent peaks at ~16.4 ka and ~15.8 ka in Chiloé Continental. A subsequent rise in CHAR drove a shift to an interglacial mode of fire activity at regional scale between ~13.1–12.5 ka ([Fig. 5](#)). In the case of Chiloé Continental, this rise culminated in a significant peak at ~12.5 ka. A modest decline in regional fire activity ensued, with variable magnitudes and sign of

anomalies among sectors between ~12.5–11.3 ka. This gave way to a rise that reached positive anomalies between ~11.3–8.1 ka, with significant high values between ~10–9.4 ka supported by Circular Block Bootstrapping and Regime Shift Detection (RSD) analyses (Rodionov, 2004) (Figs. 5 and 9). The timing for these maxima is nearly identical in the Chilean Lake District and Isla Grande de Chiloé, in contrast to Chiloé Continental which shows non-significant maxima during the early Holocene.

Regional fire activity (NWP\_CHACC) declined between ~9.4–4.8 ka to the lowest negative anomalies during the Holocene (Fig. 5). A steady multi-millennial rise started at ~4.8 ka and led to predominance of significant high values between ~3.1 ka and the present, with prominent maxima at ~4.4 ka, ~1.6 ka, ~1.1 ka, and ~0.3 ka. This multi-millennial rise is present in all studied sectors within NWP; the Chiloé Continental sector, however, does not show significant peaks between ~4.2–0.2 ka (Fig. 5). Shared peaks are evident between the Chilean Lake District and Isla Grande de Chiloé (~1.1 ka), and between Isla Grande de Chiloé and Chiloé Continental (~4.4 ka). The most recent two millennia at NWP scale feature a prominent rise that led to a broad maximum between ~3.1–0.9 ka, according to RSD (Fig. 9), that gave way to a conspicuous low between ~0.9–0.5 ka, and an increase that reached significant peaks at different times during the last ~450 years, depending on the sector.

When segregated in clusters of sites located adjacent (AND\_CHACC) and distal (WUE\_CHACC) to the Andes Cordillera, we observe similar distribution of CHAR magnitudes over the last ~18,000 years (Fig. 6). Raw CHAR values from sites adjacent to the Andes are significantly higher than distal sites over the last ~18,000 years (Supplementary Fig. 11). Although both series show a common multi-millennial structure of changes, we note millennial and centennial-scale divergences that illustrate the role of explosive volcanism as a potential trigger or modulator of climate-driven fire activity in the mountainous sectors of the Chilean Lake District and Chiloé Continental. It follows from this discussion that, in the absence of frequent explosive volcanism on the Western Upwind Environments, fire activity over the last ~18,000 years has been driven solely or primarily by climate change.

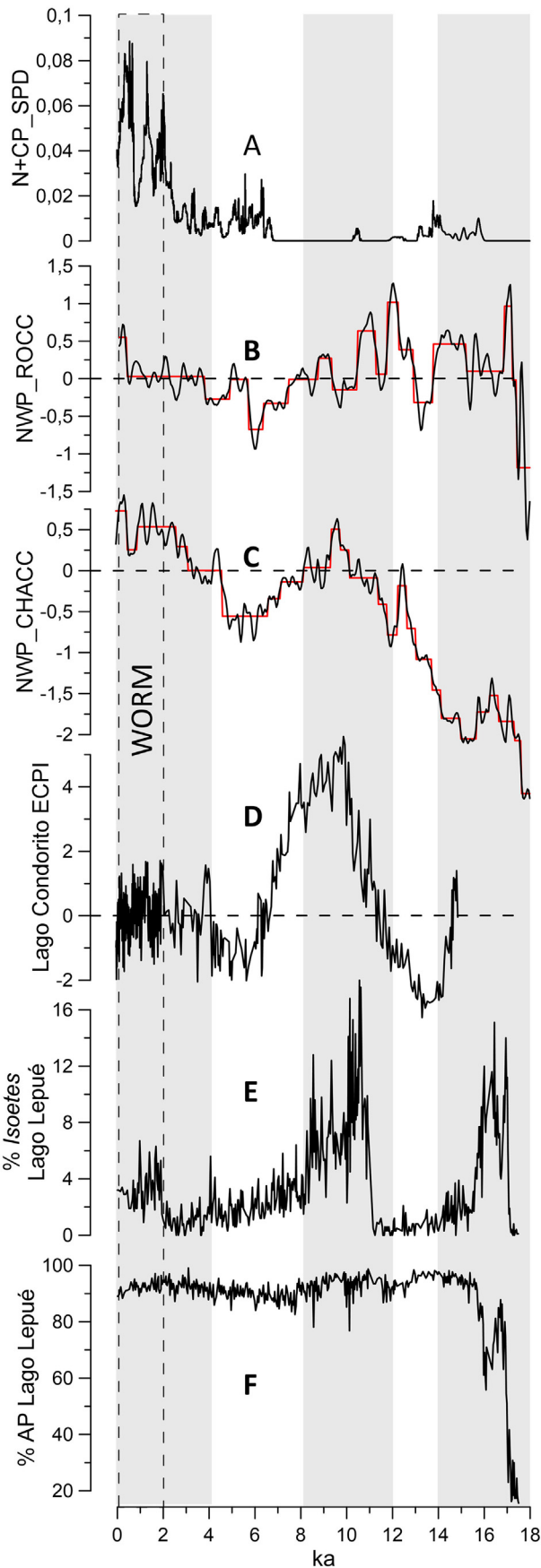
Axis 1 of a Detrended Correspondence Analysis (DCA) ordination applied to the macroscopic CHAR and tephra frequency (TF) time series younger than ~12.8 ka (Fig. 4) captures a west (Isla Grande de Chiloé sites) to east (Chiloé Continental sites) increase in TF, accounting for 43.7% of the variance. DCA Axis 2 accounts for 15.4% of the variance whose ordination may be rather meaningless given the proportionally low eigenvalue of Axis 2 and the possible “arch effect”, which is a statistical artifact and not a reliable ordination to interpret (ter Braak and Prentice, 1988). However, the choice of using the DCA approach over other simple ordination methods allows us to maximize the variance captured along Axis 1. These results allow visualization of the temporal evolution of the CHAR and TF series, in which we note a right to left progression along Axis 1, with an irreversible transition at ~6.2 ka. This points to the differing evolution of explosive volcanism in NWP since ~12.8 ka. We can visualize (Fig. 4, Supplementary Fig. 3) that the ~11 ka tephra shared among all sites in Isla Grande de Chiloé coincides with large magnitude fire events in these sites at that time, with the nuance that this event is secondary in CHAR magnitude for the sites furthest from eruptive centers (L. Huillin, L. Quilque) (Supplementary Table 1, also seen in Fig. 3), which display their CHAR maxima after ~6.2 ka. Likewise, we may note a mid-to-late Holocene progression in TF maxima along Axis 2, with a pivot point at ~2.9 ka, characterizing the evolution of explosive events in the Chilean Lake District and Chiloé Continental sectors, whose TF maxima do not necessarily correlate with CHAR maxima.

#### 4.2. Spatial and temporal ROC patterns

The ROC parameter quantifies the magnitude and rapidity of changes in the pollen stratigraphy and, as such, can be used to examine the dynamism of the former vegetation in response to past environmental change and internal dynamics within the forest communities. Unsurprisingly, the ROC data are highly variable in space and time among NWP sites since ~18 ka, considering that site selection was carried out with the aim of maximizing the local signal in small closed-basin lakes. In general, we find consistently high values in the northern Chilean Lake District sites and consistently low values in Isla Grande de Chiloé (Supplementary Figs. 1, 3, 4). The Chiloé Continental sector features the most heterogeneous results, with highest ROC values at its northern limit, and the lowest values at sea level and east of the Andean divide. We observe that raw ROC is significantly higher in the Chilean Lake District, intermediate in Isla Grande de Chiloé and significantly lower in Chiloé Continental since ~18 ka (Supplementary Fig. 10). These results suggest that high annual temperature and enhanced temperature and precipitation seasonality in the northern sector of NWP drove higher fire activity over the last ~18,000 years, accounting for significantly higher rates of vegetation change, reflective of a highly dynamic or unstable vegetation and landscape evolution.

All NWP sites are located in sectors covered by piedmont glacier lobes during the Last Glacial Maximum (LGM) and, thus, have the potential to capture rapid vegetation changes related to the colonization of recently deglaciated terrains following T1. The timing for the onset of local ice-free conditions varies among sectors, occurring first in the Chilean Lake District and western Isla Grande de Chiloé, followed by northern Chiloé Continental, next in eastern Isla Grande de Chiloé, then central Chiloé Continental, and last in southern Chiloé Continental (Denton et al., 1999; Moreno, 2020; Moreno et al., 2021b, 2022). ROC maxima attributable to primary and secondary succession processes in formerly ice-covered sectors are evident in IGC\_ROCC and CC\_ROCC between ~18–15 ka (Fig. 5). This is evident as the statistically highest multi-millennial ROC interval in the corresponding compilations between ~18–14 ka and, to a lesser extent, between ~14–12 ka (Fig. 5). The ROC compilation from the Chilean Lake District over those intervals attain the significantly highest (~14–12 ka) and lowest values (~18–14 ka), probably because forest or woodland vegetation was already present along the western margin of the Patagonian Ice Sheet during the LGM in close proximity to the study sites, allowing the instantaneous expansion and establishment of woody vegetation immediately after the onset of T1 (Henríquez et al., 2021a; Moreno et al., 2018a).

As previously discussed, a gradient in the recurrence and thickness of tephra layers is evident along a west-east and south-north transects (Fig. 3), establishing gradients for the probability of vegetation changes triggered directly or indirectly by explosive volcanism. We note that raw ROC values over the last ~18,000 years are significantly higher in Western Upwind sites (Supplementary Fig. 12). The most prominent divergences between AND\_ROCC and WUE\_ROCC occur between ~17.5–17 ka, ~16.3–16.2 ka, ~12.3–11.9 ka, ~10.3–9.6 ka, and at ~8.2 ka, during intervals of non-significant compilation variations. These divergences account for the weak correlation between these data sets over the last ~18,000 years (Fig. 6, Supplementary Table 2). If we focus the analysis on sectors within the same latitudinal range, climate, and vegetation zone, the IGC\_ROCC and CC\_ROCC exhibit a moderate correlation ( $r: 0.46$ ) since ~18 ka (Supplementary Fig. 1, Supplementary Table 2).



#### 4.3. Human occupations, CHAR, and ROC patterns

Our analysis reveals two temporal clusters in the archaeological record: a Late Pleistocene and a mid-to-late Holocene interval, separated by a gap in human occupations between ~10–6.5 ka. The former is defined by a few intensely dated archaeological localities in the Chilean Lake District (~16–13 ka) (Fig. 8), which markedly diminishes to two individual dates spanning the earliest portion of the Holocene (~12–10 ka). The mid-to late Holocene features dominance of coastal archaeological sites with an initial intermittent phase between ~6.5–2.5 ka, and a decisive increase that culminated in prominent maxima at ~2 ka, ~1.2 ka, and ~0.5 ka. The interval ~2–0 ka features the highest abundance and ubiquity of radiocarbon-dated archaeological sites throughout northwestern and central-west Patagonia; we regard this interval as a widespread occupational radiocarbon maximum in the regional dataset. This increase coincides with a diversification in site types, the prominence of bioanthropological record, and the extensive distribution of the archaeological record across the landscape (Reyes, 2020).

At centennial scale we observe a prominent decline in the dated archaeological record between ~1.2–0.8 ka that preceded a conspicuous decline in fire activity between ~0.9–0.5 ka (Figs. 6 and 8). A subsequent rise in the dated archaeological record between ~0.8–0.5 ka led to a plateau between ~0.5–0.35 ka, contemporaneous with a rise in fire activity that culminated between ~0.35–0.1 ka, which was contemporaneous with (i) the arrival of European/Chilean settlers to NWP, (ii) the sudden and ubiquitous appearance of non-native plants in pollen records from NWP starting at ~0.35 ka, and (iii) peak rates of vegetation change.

We note low frequency or absence of dated occupational events (N+CP\_SPD) between latitudes ~40°S and 46°S over an extended interval that includes significantly low fire activity (~18–13 ka), an abrupt increase (~13–12 ka), and significantly high fire activity (~10–9.4 ka) (Figs. 6 and 8). Discontinuous occupational events between ~6.5–2.5 ka, mainly coastal archaeological sites, correspond in timing with a multi-millennial rise in fires and rates of vegetation change (Fig. 8). We expect the probability of initiation and propagation of fires set by humans to increase with population size because native populations shifted from a hunter-fisher-gatherer lifeway to a less mobile dispersed settlement pattern which integrated gathering and slash and burn horticulture during the last two millennia, specially in continental locations (Aldunate, 1996). This is reflected in a shift toward moderate/strong correlations between N+CP\_SPD and compilations of macroscopic charcoal and rates of vegetation change (NWP\_CHACC, IGC\_CHACC, WUE\_CHACC, NWP\_ROCC, WUE\_ROCC, CLD\_ROCC) during the most recent ~4000 years.

Fire-history sites and most coastal archaeological sites are located in a hyperhumid maritime region, in most cases at considerable distances upwind from active volcanic centers (Isla Grande de Chiloé >100 km), aspect that minimizes or precludes the potential incendiary and disturbance effect of tephra fallout. Some lake records from Isla Grande de Chiloé (Lago Tarumán, L. Lepué) show a single cm-thick tephra deposited at ~2.3 ka, contemporaneous and potentially linked to a significant peak in the

**Fig. 9.** Compilation of (A) radiocarbon-dated archaeological sites in northwestern and central-west Patagonia (N + CP\_SPD), (B) rates of change (NWP\_ROCC) and (C) macroscopic charcoal accumulation rates (NWP\_CHACC) from northwestern Patagonian sites, along with (D) the *Eucryphia/Caldcluvia* to *Podocarpaceae* index (ECPI) from Lago Condorito, (E) the percent abundance of *Isoetes* from Lago Lepué, and (F) Arboreal Pollen sum from Lago Lepué. The red lines correspond to the weighted means of a Regime Shift Detection Algorithm applied to the NWP\_CHACC and NWP\_ROCC series. The gray and white ribbons mark the boundaries of the multi-millennial intervals examined throughout the main text. (For interpretation of the references to colour in this figure legend, the reader is referred to the Web version of this article.)

macroscopic charcoal compilations (IGC\_CHACC and NWP\_CHACC) (Figs. 5 and 6). The absence of tephra layers deposited since then, however, can hardly account for the statistically significant positive observed in those compilations between ~1.8–0.9 ka, and during the last ~500 years. The widespread presence of radiocarbon-dated occupations along the continental coasts and in the Archipiélago de Chiloé and A. de los Chonos, suggests a potential human trigger for ignitions over the last ~2400 years, either as the result of neglected fireplaces, or purposefully as suggested by the use of the more recent slash and burn strategy. The discovery of microfossils of *Phaseolus vulgaris*, *Solanum tuberosum*, and *Zea mays* in the dental calculus of individuals confirms the introduction of domesticated plants, and to some extent horticulture, in Isla Grande de Chiloé and Archipiélago de los Chonos over the last 500 years (Belmar et al., 2021). Though these acted as a complement to marine-based diets, they highlight the extent of human modification of the environment in the latest part of the record.

The marked absence of archaeological dated sites during the early Holocene (~12–8 ka) (N+CP\_SPD) must be regarded as preliminary given the lack of a systematic, regionally oriented archaeological research strategy (Campbell and Quiroz, 2015), and the fact that study efforts have been put into few thoroughly investigated old sites. This absence during the early Holocene fire maximum may imply that forest fires were initiated by non-human factors, underscoring the importance of lightning strikes and explosive volcanism as the primary ignition agents during a pan-Patagonian SWW minimum (~11–7.8 ka) (Moreno et al., 2021a). Though plausible and consistent with the results and analyses shown in this paper, this “absence of evidence is evidence of absence” interpretation rests on the assumption that the archaeological record is homogeneous and representative of all sectors and millennia in NWP since ~18 ka. Campbell and Quiroz (2015) attributed this radiocarbon gap to a historical focusing of archaeological (and radiocarbon) efforts on late Pleistocene sites from a few inland sites, and shell middens along the Pacific and Seno Reloncaví coasts, which appear distinctively after ~6.5 ka (San Román, 2014). Reyes et al. (2016) remarked that archaeological sites along the Archipiélago de los Chonos overlie deposits and geomorphic features dating to the mid-Holocene marine transgression, which reached its regional maximum at ~7 ka. This area is further affected by vertical displacement as a consequence of its proximity to the Liquiñe-Ofqui fault zone (Reyes et al., 2018). The rarity of shell middens of early Holocene age is a globally recognized phenomenon (Hale et al., 2021), the majority of sites having that age are thought to lie submerged below modern sea level or eroded by the transgressive/regressive trends during the middle Holocene. However, early Holocene shell middens in arid to semi-arid latitudes of north-central Chile are a common feature, especially at elevated terraces that were not exposed to sea level rise (Jackson et al., 2012; Méndez, 2013). We note that the sea level preservation constraint also applies to sites in the Chilean Lake District, Isla Grande de Chiloé, and Chiloé Continental, accounting for the widespread absence of early Holocene coastal sites. Hence, we think that the scarcity of radiocarbon-dated archaeological sites between ~12–6.5 ka in NWP might represent an artifact of sampling biases brought by a site-focused research strategy on inland records, as well as the low preservation potential in coastal sectors throughout the region.

Our results suggest that the magnitude of fire activity since the onset of European invasion (~0.4 ka) matches pre-European maxima between ~1.7–1.5 ka and ~1.1–1 ka (Fig. 10), and these constitute the largest-magnitude centennial-scale events in the entire record. The European peak has values ~33% higher than the highest significant positive anomaly during the early Holocene. These results are consistent with the expectation that human

activities facilitated or exacerbated the potential for natural fire occurrence at regional scale, as a function of population density or sedentarism.

#### 4.4. Regional and sub-continental comparisons

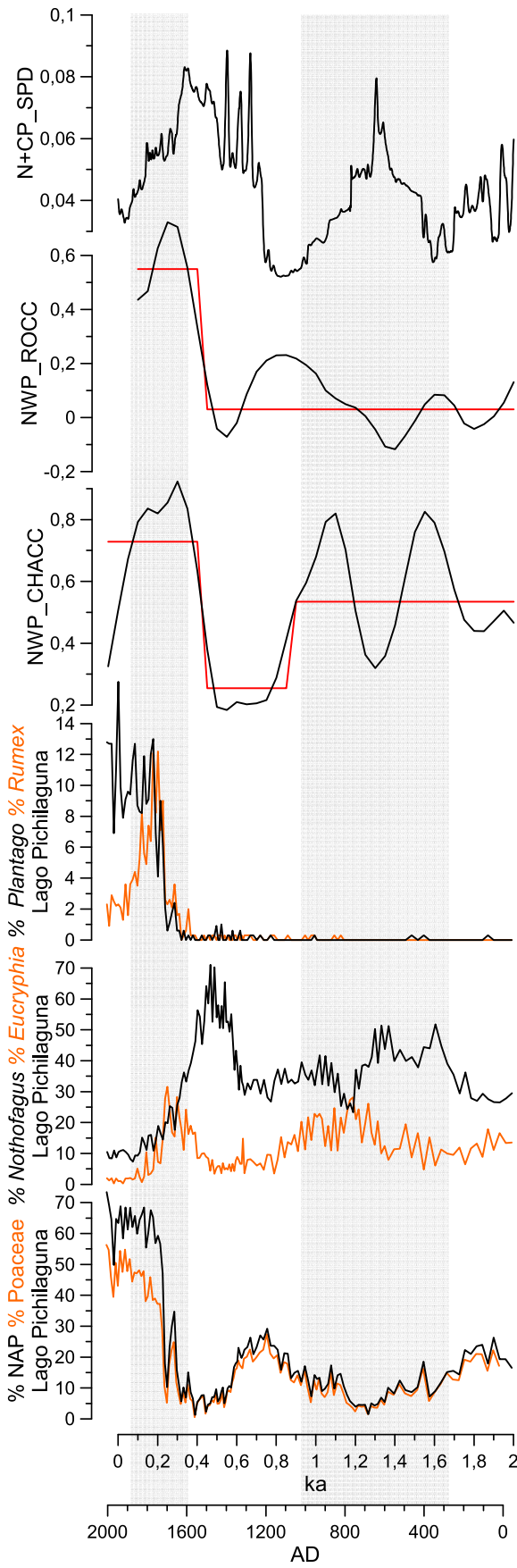
The regional (NWP\_CHACC) and sub-continental (TSA\_CHACC) (Fig. 7) charcoal compilations are strikingly similar in general trends over the last ~18,000 years, with noteworthy differences:

1. The magnitude of negative anomalies in NWP\_CHACC during T1 is much larger than in TSA\_CHACC and persist uninterrupted between ~18–13.1 ka.
2. The magnitude of positive anomalies during the early Holocene is much larger in TSA\_CHACC, and these persist over a longer interval than in NWP\_CHACC.
3. Statistically high values in TSA\_CHACC occur only between ~11.7–8.9 ka, whereas in NWP\_CHACC these take place between ~10–9.4 ka, at ~8.3 ka, and prevail between ~3.1 ka and the present.

Important differences in the geographic, climatic, vegetation composition and physiognomy, stratigraphic, and taphonomy contexts, as well as the methodologies underlying the data sources are worth considering when assessing similarities and differences among these charcoal compilations:

- a) TSA\_CHACC includes a vegetation and climatically heterogeneous region throughout northern, central, and southern Patagonia, east and west of the Andes and, thus, integrates in a single curve the evolution of fire regimes that might be contrasting, opposite, time-transgressive or, simply put, different. In contrast, the records included in NWP\_CHACC monitor areas adjacent and west of the Andean divide between ~44°S and 40°S.
- b) TSA\_CHACC includes charcoal records from bogs and fens that tend to yield charcoal records that exacerbate the local signal in detriment of an extra-local or regional signal. Furthermore, some mires were lakes that terrestrialized at different moments over the last ~18,000 years, changing their landscape-sensing capability throughout the record. In contrast, 14 of the 15 records included in NWP\_CHACC were retrieved from small-closed basin lakes with constant lacustrine sedimentation.
- c) TSA\_CHACC includes microscopic and macroscopic charcoal records some of which were produced using different procedures and analytical methods. In contrast, the accumulation-rate records included in NWP\_CHACC were derived from piston cores from small-closed basin lakes and feature contiguous/continuous macroscopic charcoal counts and were processed and analyzed following the same exact protocols.
- d) The continuity and time resolution of records included in TSA\_CHACC is variable, having median time resolution between 6 and 342 years between samples. In contrast, the records included in NWP\_CHACC feature continuous/contiguous records with median time resolution values between samples in the range between 14 and 54 years.

A combination of the taphonomic and analytical differences mentioned above could account for the divergences between NWP\_CHACC and TSA\_CHACC over the last ~18,000 years. Alternatively, there might be genuine NWP-specific fire histories resulting from a unique combination of environmental factors along north-south and east-west transects. We note that the



timing, persistence, and mobility of indigenous inhabitants, along with their technology and population densities constitute additional sources of environmental variability at the landscape scale.

Our regional rates of change compilation (NWP\_ROCC) resembles the “temperate South American” compilation reported by Mottl et al. (2021a), which shows a gradual and steady decline in ROC between ~18–3 ka followed by an equally gradual and low magnitude increase toward the present. These low-frequency features, however, contrast with the millennial/centennial-scale reversals and intensifications evident in NWP\_ROCC, that include prominent statistically significant maxima between ~17.2–17 ka, ~12.3–11.9 ka, ~11.2–10.9 ka, and ~0.3 ka (Fig. 6). The source for these differences might relate to the diversity of taphonomic and analytical approaches present in the “temperate South American” compilation, the time resolution of those records, the choice of the binning window (500 versus 250), the large-scale climatic and vegetation heterogeneities found along the broad region analyzed by Mottl et al. (2021a), and differences in the magnitude and frequency of explosive volcanic events (see below).

#### 4.5. Climatic and ecologic implications

Variability in fire activity is evident from multi-decadal to multi-millennial timescales throughout NWP, aspect we interpret as changes in the recurrence, magnitude, and duration of hydroclimate anomalies (that is, coupled warm/dry or cold/wet anomalies). This interpretation relies on the modern climatic controls on fire occurrence in the hyperhumid ecosystems of western Patagonia and the regional dominance of rainforest vegetation since T1 (Henríquez et al., 2021a, 2021b; Holz et al., 2012; Holz and Veblen, 2009; Moreno and Videla, 2016; Urrutia-Jalabert et al., 2018). Hydrologic variability in this sector is highly dependent upon changes in the intensity of the SWW impinging upon the austral Andes which in turn is controlled by their position and intensity through the annual cycle. We note that the *Eucryphia/Caldcluvia* to Podocarpaceae Index (ECPI) from Lago Condorito, a paleovegetation ratio that captures multi-millennial scale changes in hydrologic balance in NWP since ~14 ka (Figs. 2 and 9), shows moderate correlation with NWP\_CHACC ( $r: 0.44$ ) and WUE\_CHACC ( $r: 0.45$ ), and strong with CLD\_CHACC ( $r: 0.66$ ) (Supplementary Table 9) over the last ~14,000 years. The degree of association is higher in all sectors between ~14–12 ka (NWP\_CHACC: 0.75, WUE\_CHACC: 0.56, CLD\_CHACC: 0.82), and in the northern (CLD\_CHACC: 0.82) and western (WUE\_CHACC: 0.72) sectors between ~12–8 ka (Supplementary Tables 4, 5). The correlation declines between ~8–4 ka (NWP\_CHACC: 0.41, WUE\_CHACC: non-significant, CLD\_CHACC: 0.5) and becomes non-significant or moderate negative (CC\_CHACC: -0.35, AND\_CHACC: -0.33) between ~4–0 ka (Supplementary Figs. 3–6). Superimposed upon this primary control, human activities have modulated the occurrence of fires, through land-use changes and ignition. The fact that ECPI and macroscopic charcoal compilations decouple between ~4–0 ka and, conversely, the correlations between the N+CP\_SPD of radiocarbon-dated archaeological sites with macroscopic charcoal and rates-of-change compilations turned moderate positive over the same interval, are consistent with a growing importance of human activities as drivers of fires and rates of vegetation change in NWP over the last ~4000 years.

The most prominent increase in the macroscopic charcoal compilations started at ~13.1 ka and culminated with a peak at

**Fig. 10.** Detail of Fig. 9 spanning the portion of the record between ~2 ka and the present. The curves shown in the lower half are selected plant taxa from the Lago Pichilaguna pollen record published by Moreno et al. (2018a). The vertical gray ribbons mark the timing of significant NWP\_CHACC maxima.

~12.5 ka (Fig. 9). This shift preceded abrupt increases in shade-intolerant trees (*Weinmannia trichosperma*) (Fig. 11) and Non-Arboreal Pollen (chiefly Poaceae) in multiple sites throughout NWP (Moreno et al., 2021b), attesting to widespread stand-replacing fires throughout the region. These events occurred at the onset of the Younger Dryas stadial in the northern hemisphere (Alley, 2000) and a rise in atmospheric temperatures and CO<sub>2</sub> concentrations in Antarctic ice cores (Monnin et al., 2001) (Fig. 11). Regional explanations for the abrupt fire shift include a southward shift of the SWW, in the context of interpreted cooling (Henríquez et al., 2021a; Massaferro et al., 2009, 2014; Moreno, 2000; Moreno et al., 2001, 2012) or slight warming (Moreno, 2020), and/or human-set fires (Heusser, 1994, 2003; Moreno, 2000; Moreno et al., 2001). We posit that the ~13.1 ka shift marks the onset of an interglacial mode of fire activity driven by a decline in SWW influence which led to enhanced precipitation seasonality in NWP. One study from the Pilauco site (Pino et al., 2019) found discrete increases in charcoal, peak concentrations of platinum, high-temperature spherules, meltglass, and nanodiamonds at ~12.77 ± 0.16 ka, and attributed these changes to a cosmic impact. From a regional perspective, we note that the NWP\_CHACC dataset shows a multi-millennial increase in CHAR that started at ~15.8 ka and accentuated at ~13.1 ka, ~3000 and ~300 years before the putative cosmic layer, respectively (Fig. 9). The timing and significance of this accentuation is supported by the RSD calculated on the compiled CHAR means. The discrete accentuation was followed by a sustained ~4500-year long interval of heightened fire activity. These aspects are not compatible with a single, discrete, short-lived, extra-terrestrial trigger pinpointed at ~12.8 ka, unless multiple cosmic impacts are advocated as triggers for the multiple centennial and millennial-scale increases in regional fire activity after ~13.1 ka. Future analyses will determine the regional significance of the putative cosmic impact as a driver for the onset of an interglacial mode of fire activity, and whether the observed differences in age with the onset of biomass burning at regional scale fall within or outside the dating and age-model confidence intervals.

Besides the climatic influence on the time evolution of fire occurrence and rapid vegetation change in NWP, we observe that explosive volcanism stands as an equally important driver of divergences between Western Upwind Environments and sites located near active volcanic centers in the NWP Andes. We posit that this aspect, on its own or in combination with the advection of Atlantic-sourced moisture to the eastern Andean slopes (Agosta et al., 2015; Gilli et al., 2001; Jara et al., 2019; Quade and Kaplan, 2017), could account for the divergences in timing, rate, and direction of vegetation and fire histories from the Pacific and Atlantic flanks of the northern Patagonian Andes (Iglesias and Whitlock, 2014; Jara et al., 2019; Mottl et al., 2021a; Nanavati et al., 2019). This influence is exacerbated when considering that the bulk of volcanic plumes from Patagonian eruptive centers are primarily deflected east of the Andes by the prevailing SWW.

Positive anomalies in fire activity between ~10.6–8.1 ka at regional scale (NWP\_CHACC) correspond in timing with a low lake-level interval and widespread abundance of pollen from tree species characteristic of the Evergreen Valdivian Rainforest in NWP, captured by increased abundance of littoral macrophytes and positive ECPI values (Fig. 9), indicating warm and dry conditions during a minimum in SWW strength over NWP (Fletcher and Moreno, 2011, 2012; Moreno et al., 2010, 2021a). A subsequent decline in fire activity led to the lowest negative anomalies during the Holocene at ~6 ka, coeval with a rise in lake levels and increase in cold-tolerant conifers characteristic of the Evergreen North Patagonian rainforest, expressed as a decline that led to negative ECPI values (Fig. 9). These data suggest that cold-temperate and wet

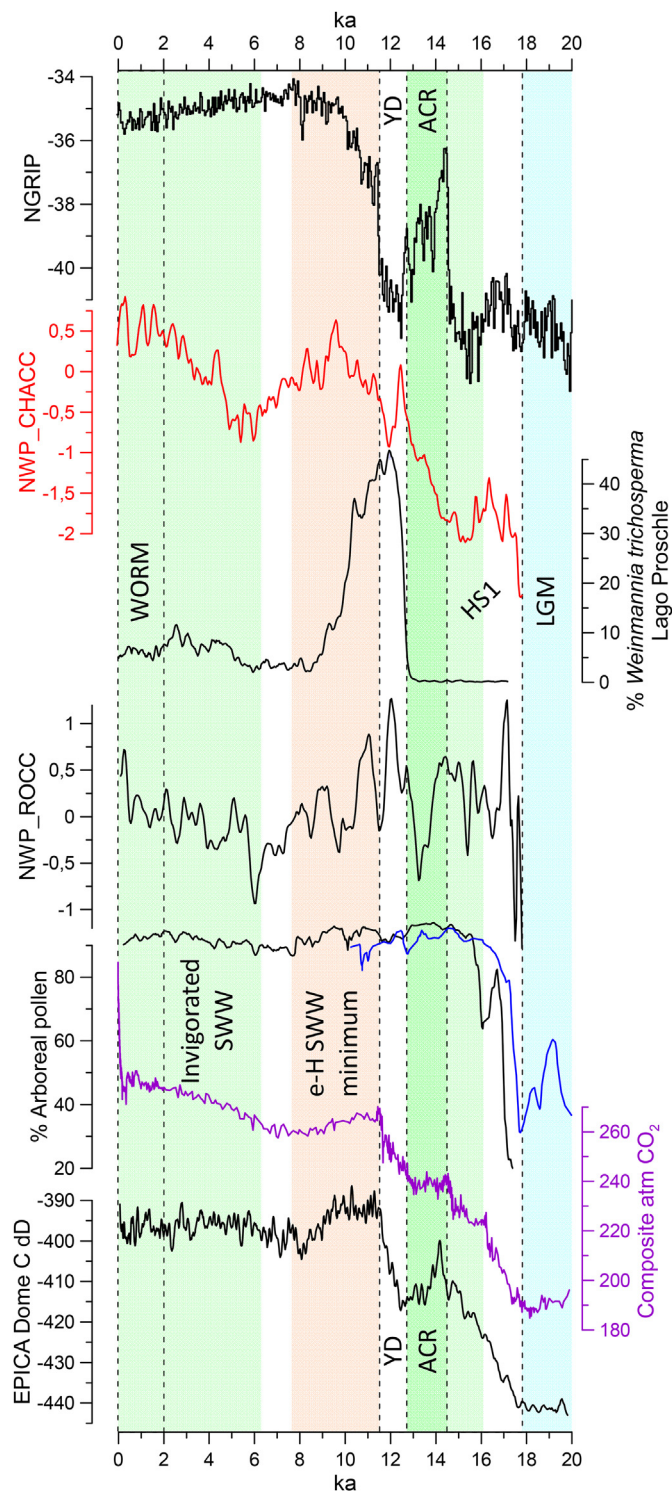


**Fig. 11.** Comparison of the Rates of Change compilation (NWP\_ROCC) and macroscopic charcoal accumulation rates compilation (NWP\_CHACC) from northwestern Patagonian sites with ice core data from Greenland (NGRIP δ<sup>18</sup>O) and Antarctica (EPICA Dome C δD, atmCO<sub>2</sub>). We also include the smoothed percent abundance of *Weinmannia trichosperma* from Lago Proschle and the Arboreal Pollen sum from Lago Lepué (black) and Canal de la Puntilla (blue). LGM = Last Glacial Maximum, HS1 = Heinrich Stadial 1, ACR = Antarctic Cold Reversal, YD = Younger Dryas, WORM = Widespread Occupational Radiocarbon Maximum. The light blue vertical ribbon represents cold/hyperhumid conditions during the Last Glacial Maximum (LGM), the green ribbons represent cool-temperate and wet conditions, and the orange ribbon represents warm/relatively dry conditions during the early Holocene. The darker green ribbon represents colder and wetter conditions than the ~16.3–14.8 ka interval. (For interpretation of the references to colour in this figure legend, the reader is referred to the Web version of this article.)

conditions, brought by invigorated SWW at regional and zonal scale, reduced fire activity in NWP. Renewed fire activity ensued, culminating in the largest-magnitude positive anomalies of the entire record during the last two millennia. Unlike the early Holocene portion of the NWP record, the late Holocene does not feature a distinct multi-millennial scale warm/dry anomaly. Instead, recent studies in the region have detected a pervasive centennial-scale pulsing of warm/dry events which alternate with cold/wet intervals since ~5.3 ka (Moreno and Videla, 2016) or ~6.5 ka (Henríquez et al., 2021b). These have been attributed to changes in SWW influence at regional scale brought by Southern Annular Mode-like and/or El Niño Southern Oscillation-like variability at centennial timescale, which produced megadroughts that exacerbated fire activity.

The most recent two millennia feature the largest-magnitude peaks in fire activity between ~1.7–0.9 ka, a reversal between ~0.9–0.5 ka, and a recovery between ~0.5 ka and the present (Fig. 10). The latter increase is related to peak rates of vegetation change driven by abrupt deforestation (increase in Non-Arboreal pollen -chiefly Poaceae-, declines in *Nothofagus* and *Eucryphia*) and spread of invasive exotic species of European origin (*Plantago* and *Rumex*) (Fig. 10), and a shift to a warm/dry centennial-scale phase in the Chilean Lake District (Henríquez et al., 2021b; Moreno and Videla, 2016; Moreno et al., 2018a; Sepúlveda-Zúñiga et al., 2022), contemporaneous with historical evidence for the onset of European/Chilean settlement (Otero, 2006). Our results diverge from those reported by Power et al. (2013), who found a biomass-burning decline that started at AD 1500 (~0.45 ka), based on charcoal compilations based on records retrieved from the Global Paleofire Database from multiple sectors of South, Meso, and North America. This biomass burning decline in the Americas was explained in climatic terms by a cooling event during the Little Ice Age (Power et al., 2013), which was contemporaneous with an inferred native population decline between AD 1500–1700 (~0.45–0.25 ka) throughout the Americas. The results of our analysis of the NWP data diverges from these premises, considering that the macroscopic charcoal compilations and summed probability density of radiocarbon-dated archaeological sites reached significantly high values starting at AD ~1200 (~0.75 ka) and at AD ~1500 (~0.4 ka), respectively. We posit that enhanced fire activity in NWP starting at ~0.4 ka (Fig. 10) resulted from a negative hydrologic balance phase brought by a southward shift of the SWW during the Little Ice Age and subsequent burning by European/Chilean settlers (Henríquez et al., 2021a, b; Moreno et al., 2018a; Moreno et al., 2018b). This interpretation, however, differs from Bertrand et al. (2014)'s reconstruction of reduced precipitation seasonality in central-west Patagonia brought by a northward shift of the SWW during the last ~500 years, based on a sediment core obtained from Quitrailco fjord (~46°S). We note that the regional significance of this record awaits replication, ideally from sectors unaffected by the direct influence of meltwater plumes from glaciated valleys, and fluvial discharge from active volcanic centers.

## 5. Conclusions

In this section we summarize the results of this paper in the context of the questions posed in the introduction.

- 1 Is there a consistent temporal fire activity trend in NWP since ~18 ka? At multi-millennial scale we detect a significant low in fire activity between ~18–13.1 ka, an abrupt rise between ~13.1–12.5 ka, and fire activity above the Holocene mean between ~10.6–8.1 ka with significant high values between ~10–9.4 ka. A steady decline ensued reaching the lowest Holocene values between ~6–5.4 ka, superseded by an increase

that led to significant high values between ~3.1 ka and the present.

- 2 How did fire activity vary along a north-south transect and Andean/Western Upwind Environments in the region? Our analysis reveals that the magnitude of raw macroscopic charcoal accumulation rates follows modern gradients in precipitation and explosive volcanism in NWP, underscoring the role of climate and disturbance regimes, related to explosive volcanism, as the primary controls of fire occurrence at regional scale.
- 3 Are we able to distinguish unsynchronized localized eruption-induced fire activity from more regionally synchronous climate-induced fire activity? Macroscopic charcoal records from sites located in Andean and Western Upwind Environments share a multi-millennial structure of fire activity since ~18 ka, overprinted by millennial and centennial-scale divergences. Sites located closest to the Andean eruptive centers contain a larger number and thickness of tephra layers, which are known to trigger vegetation changes and generate dead biomass susceptible to ignition. These divergences underscore the role of explosive volcanism as a trigger or modulator of climate-driven fire activity in the vicinity of active eruptive centers.
- 4 Did fire activity influence the rates of vegetation change (or vice versa) at regional scale? We observe the highest covariation between compilations of macroscopic charcoal accumulation rates and rates of vegetation change between ~14–12 ka and ~4–0 ka, suggesting enhancements in the fire-vegetation-climate coupled system. These intervals correspond in timing with important changes in moisture delivered by the Southern Westerly Winds.
- 5 How did fire activity vary in relation to changes in southern westerly wind influence? and in relation to the temporal distribution of human occupations in the region? Fire activity covaries with changes in the Lago Condorito *Eucryphia/Caldcluvia* to *Podocarpaceae* pollen Index (ECPI) estimate of hydrologic balance over the last ~14,000 years. The strength of this correlation is maximal between ~14–12 ka, diminishes toward ~4 ka and reaches non-significant values since then. These results underscore the importance of SWW influence on wildfires at millennial and multi-millennial timescales, and the limitations of the Lago Condorito ECPI to capture wildfire variability since ~4 ka. The most recent millennia feature a major increase in the occurrence of radiocarbon-dated archaeological sites, raising the possibility that human activities, purposefully or accidentally, contributed to heightened fire occurrence during an interval characterized by centennial-scale hydroclimate variability. Fire activity and the rates of vegetation change peaked during the last ~450 years driven by large-scale deforestation and land-use changes associated with European-Chilean settlement.

## Author contributions

P.I. Moreno conceived the concept for this study, wrote the manuscript, developed the stratigraphic records with students C.A. Henríquez, J. Videla, and E.I. Fercovic. L. Villacís carried out the compilations and statistical analyses. C. Méndez and O. Reyes developed some of the archaeological records reviewed in this study and developed the synthesis of radiocarbon-dated sites, B.V. Alloway studied the volcanic sediments and contributed with their interpretation and integration in this study. R. Villa-Martínez participated in numerous field seasons, helped students in laboratory analyses and thesis work. All authors provided insights, discussion, and participated in editing the manuscript.

## Declaration of competing interest

The authors declare that they have no known competing financial interests or personal relationships that could have appeared to influence the work reported in this paper.

## Data availability

Data will be made available on request.

## Acknowledgements

We thank R. Flores, P. Ugalde, and R. Soteres for help during field work, L. Hernández for laboratory assistance, and T. Gilderson, J. Southon, R. de Pol for acquisition of radiocarbon dates. We thank R. Garreaud for constructive comments on the modern climate and paleoclimate interpretation sections, and W. Nanavati for insightful and constructive comments to the original submission. We acknowledge funding from ANID FONDECYT grants 1191435, 1171773, 1210045, 1210042, FONDAP 15110009, the ANID Millennium Science Initiative/Millennium Nucleus Paleoclimate NCN17\_079, ANID Regional R20F0002, M. Sc. Fellowship 22172359, Ph.D. Fellowship CONICYT #21161417 and 21140039.

## Appendix A. Supplementary data

Supplementary data to this article can be found online at <https://doi.org/10.1016/j.quascirev.2022.107899>.

## References

- Adán, L., Mera, R., Navarro, X., Campbell, R., Quiroz, D., Sánchez, M., 2016. Historia prehispánica en la región Centro-Sur de Chile: cazadores-recolectores holocénicos y comunidades alfareras (ca. 10.000 años a.C. a 1.550 años d.C.). In: Falabella, F., Sanhueza, I., Aldunate, C., Hidalgo, J. (Eds.), *Prehistoria en Chile, desde sus primeros habitantes hasta los Incas*. Editorial Universitaria, Santiago, pp. 401–441.
- Agosta, E., Compagnucci, R., Ariztegui, D., 2015. Precipitation linked to Atlantic moisture transport: clues to interpret Patagonian palaeoclimate. *Clim. Res.* 62, 219–240.
- Aguayo, R., León-Muñoz, J., Vargas-Baeheler, J., Montecinos, A., Garreaud, R., Urbina, M., Soto, D., Iriarte, J.L., 2019. The glass half-empty: climate change drives lower freshwater input in the coastal system of the Chilean Northern Patagonia. *Climatic Change* 155, 417–435.
- Aldunate, C., 1996. Mapuche: gente de la tierra. In: Hidalgo, J., Schiappacasse, V., Niemeyer, H., Aldunate, C., Mege, P. (Eds.), *Etnografía Sociedades Indígenas Contemporáneas y su Ideología*. Editorial Andrés Bello, Santiago, pp. 111–134.
- Alley, R.B., 2000. The Younger Dryas cold interval as viewed from central Greenland. *Quat. Sci. Rev.* 19, 213–226.
- Alloway, B.V., Lowe, D.J., Barrell, D.J.A., Newnham, R.M., Almond, P.C., Augustinus, P.C., Bertler, N.A.N., Carter, L., Litchfield, N.J., McGlone, M.S., Shulmeister, J., Vandergoes, M.J., Williams, P.W., 2007. Towards a climate event stratigraphy for New Zealand over the past 30 000 years (NZ-INTIMATE project). *J. Quat. Sci.* 22, 9–35.
- Alloway, B.V., Moreno, P.I., Pearce, N.J.G., De Pol-Holz, R., Henriquez, W.I., Pesce, O.H., Sagredo, E., Villarosa, G., Outes, V., 2017a. Stratigraphy, age and correlation of Lepue Tephra: a widespread c. 11 000 cal a BP marker horizon sourced from the Chaitén Sector of southern Chile. *J. Quat. Sci.* 32, 795–829.
- Alloway, B.V., Pearce, N.J.G., Moreno, P.I., Villarosa, G., Jara, I., De Pol-Holz, R., Outes, V., 2017b. An 18,000 year-long eruptive record from Volcán Chaitén, northwestern Patagonia: paleoenvironmental and hazard-assessment implications. *Quat. Sci. Rev.* 168, 151–181.
- Alloway, B.V., Almond, P.C., Moreno, P.I., Sagredo, E., Kaplan, M.R., Kubik, P.W., Tonkin, P.J., 2018. Mid-latitude trans-Pacific reconstructions and comparisons of coupled glacial/interglacial climate cycles based on soil stratigraphy of cover-beds. *Quat. Sci. Rev.* 189, 57–75.
- Alloway, B.V., Pearce, N.J.G., Moreno, P.I., Villarosa, G., Ignacio Jara, I., Henríquez, C.A., Sagredo, E., Ryan, M., Outes, V., 2022. Refinement of the tephrostratigraphy straddling the northern Patagonian Andes (40–41°S): new tephra markers, reconciling different archives and ascertaining the timing of piedmont deglaciation. *J. Quat. Sci.* 37, 441–477.
- Belmar, C.A., Reyes, O., Albornoz, X., Tessone, A., San Román, M., Morello, F., Urbina, X., 2021. Evaluando el consumo y uso de plantas entre cazadores recolectores pescadores marinos a través del estudio del tártaro dental humano en los canales septentrionales de Patagonia (41°S–47°S). *Chungará* 53, 400–418.
- Bertrand, S., Castiaux, J., Juvigné, E., 2008. Tephrostratigraphy of the late glacial and Holocene sediments of Puyehue lake (southern volcanic zone, Chile, 40°S). *Quat. Res.* 70, 343–357.
- Bertrand, S., Hughen, K., Sepúlveda, J., Pantoja, S., 2014. Late Holocene covariability of the southern westerlies and sea surface temperature in northern Chilean Patagonia. *Quat. Sci. Rev.* 105, 195–208.
- Bird, D., Miranda, L., Vander Linden, et al., 2022. p3k14c, a synthetic global database of archaeological radiocarbon dates. *Sci. Data* 9, 27. <https://doi.org/10.1038/s41597-022-01118-7>
- Blaauw, M., Christen, J.A., 2011. Flexible paleoclimate age-depth models using an autoregressive gamma process. *Bayesian Anal.* 6, 457–474.
- Blarquez, O., Vannière, B., Marlon, J.R., Daniau, A.-L., Power, M.J., Brewer, S., Bartlein, P.J., 2014. paleofire: an R package to analyse sedimentary charcoal records from the Global Charcoal Database to reconstruct past biomass burning. *Comput. Geosci.* 72, 255–261.
- Boisier, J.P., Rondanelli, R., Garreaud, R.D., Muñoz, F., 2016. Anthropogenic and natural contributions to the Southeast Pacific precipitation decline and recent megadrought in central Chile. *Geophys. Res. Lett.* 43, 413–421.
- Boisier, J.P., Alvarez-Garretón, C., Cepeda, J., Osses, A., Vásquez, N., Rondanelli, R., 2018. CR2MET: a high-resolution precipitation and temperature dataset for hydroclimatic research in Chile. In: *EGU General Assembly Conference Abstracts*, 19739.
- Cai, W., McPhaden, M.J., Grimm, A.M., Rodrigues, R.R., Taschetto, A.S., Garreaud, R.D., Dewitte, B., Poveda, G., Ham, Y.-G., Santos, A., Ng, B., Anderson, W., Wang, G., Geng, T., Jo, H.-S., Marengo, J.A., Alves, L.M., Osman, M., Li, S., Wu, L., Karapetroudi, C., Takahashi, K., Vera, C., 2020. Climate impacts of the el niño–southern oscillation on south America. *Nat. Rev. Earth Environ.* 1, 215–231.
- Campbell, R., Quiroz, D., 2015. Chronological database for Southern Chile (35°30'–42° S), ~33000 BP to present: human implications and archaeological biases. *Quat. Int.* 356, 39–53.
- Casanova, M., Salazar, O., Seguel, O., Luzio, W., 2013. *The Soils of Chile*. World Soils Book Series. Springer, Netherlands, p. 185.
- Cooper, J., Sheets, P., 2012. *Surviving Sudden Environmental Change: Answers from Archaeology*. University Press of Colorado, University Press of Colorado, Boulder, Boulder.
- Crema, E.R., Bevan, A., 2021. Inference from large sets of radiocarbon dates: software and methods. *Radiocarbon* 63, 23–39.
- Daniau, A.-L., Bartlein, P.J., Harrison, S.P., Prentice, I.C., Brewer, S., Friedlingstein, P., Harrison-Prentice, T.L., Inoue, J., Izumi, K., Marlon, J.R., Mooney, S., Power, M.J., Stevenson, J., Tinner, W., Andric, M., Atanassova, J., Behling, H., Black, M., Blarquez, O., Brown, K.J., Carcaillet, C., Colchoun, E.A., Colombaroli, D., Davis, B.A.S., D'Costa, D., Dodson, J., Dupont, L., Eshetu, Z., Gavin, D.G., Genries, A., Haberle, S., Hallett, D.J., Hope, G., Horn, S.P., Kassa, T.G., Katamura, F., Kennedy, L.M., Kershaw, P., Krivonogov, S., Long, C., Magri, D., Marinova, E., McKenzie, G.M., Moreno, P.I., Moss, P., Neumann, F.H., Norström, E., Paitre, C., Rius, D., Roberts, N., Robinson, G.S., Sasáki, N., Scott, L., Takahara, H., Terwilliger, V., Thevenon, F., Turner, R., Valsecchi, V.G., Vannière, B., Walsh, M., Williams, N., Zhang, Y., 2012. Predictability of biomass burning in response to climate changes. *Global Biogeochem. Cycles* 26.
- Davies, B.J., Darvill, C.M., Lovell, H., Bendle, J.M., Dowdeswell, J.A., Fabel, D., García, J.-L., Geiger, A., Glasser, N.F., Gheorghiu, D.M., Harrison, S., Hein, A.S., Kaplan, M.R., Martin, J.R.V., Mendelova, M., Palmer, A., Pelto, M., Rodés, A., Sagredo, E.A., Smedley, R.K., Smellie, J.L., Thorndycraft, V.R., 2020. The evolution of the Patagonian Ice Sheet from 35 ka to the present day (PATICE). *Earth Sci. Rev.* 204, 103152.
- Denton, G.H., Lowell, T.V., Heusser, C.J., Schlüchter, C., Andersen, B.G., Heusser, L.E., Moreno, P.I., Marchant, D.R., 1999. Geomorphology, stratigraphy, and radiocarbon chronology of Llanquihue drift in the area of the southern Lake District, Seno Reloncaví, and Isla Grande de Chiloé, Chile, 81A. *Geografiska Annaler Series a-Physical Geography*, pp. 167–229.
- Dillehay, T., 1989. Monte Verde. A Late Pleistocene Settlement in Chile. *Paleoenvironment and Site Context*. Smithsonian Institution Press, Washington.
- Dillehay, T.D., Ocampo, C., Saavedra, J., Pino, M., Scott-Cummings, L., Kováčik, P., Silva, C., Alvar, R., 2019. New excavations at the late Pleistocene site of Chin-chihuapi I, Chile. *Quat. Res.* 92, 70–80.
- Dillehay, T.D., Ocampo, C., Saavedra, J., Sawakuchi, A.O., Vega, R.M., Pino, M., Collins, M.B., Scott Cummings, L., Arregui, I., Villagrán, X.S., Hartmann, G.A., Mella, M., González, A., Dix, G., 2015. New archaeological evidence for an early human presence at Monte Verde, Chile. *PLoS One* 10, e0141923.
- Faegri, K., Iversen, J., 1989. *Textbook of Pollen Analysis*. John Wiley & Sons.
- Fletcher, M.-S., Moreno, P.I., 2011. Zonally symmetric changes in the strength and position of the Southern Westerlies drove atmospheric CO<sub>2</sub> variations over the past 14 k. y. *Geology* 39, 419–422.
- Fletcher, M.S., Moreno, P.I., 2012. Have the Southern Westerlies changed in a zonally symmetric manner over the last 14,000 years? A hemisphere-wide take on a controversial problem. *Quat. Int.* 253, 32–46.
- Fogt, R.L., Marshall, G.J., 2020. The southern annular mode: variability, trends, and climate impacts across the southern hemisphere. *WIREs Clim. Change* 11, e652.
- Galanter, M., Levy, H., Carmichael, G.R., 2000. Impacts of biomass burning on tropospheric CO, NO<sub>x</sub>, and O<sub>3</sub>. *J. Geophys. Res. Atmos.* 105, 6633–6653.
- Garreaud, R., Alvarez-Garretón, C., Barichivich, J., Boisier, J.P., Christie, D., Galleguillos, M., LeQuesne, C., McPhee, J., Zambrano-Bigiarini, M., 2017. The 2010–2015 mega drought in Central Chile: impacts on regional hydroclimate and vegetation. *Hydrol. Earth Syst. Sci. Discuss.* 1–37, 2017.

- Garreaud, R., Lopez, P., Minvielle, M., Rojas, M., 2013. Large-scale control on the patagonian climate. *J. Clim.* 26, 215–230.
- Garreaud, R.D., 2007. Precipitation and circulation covariability in the extratropics. *J. Clim.* 20, 4789–4797.
- Garreaud, R.D., 2018. Record-breaking climate anomalies lead to severe drought and environmental disruption in western Patagonia in 2016. *Clim. Res.* 74, 217–229.
- Garreaud, R.D., Nicora, M.G., Bürgesser, R.E., Ávila, E.E., 2014. Lightning in western Patagonia. *J. Geophys. Res. Atmos.* 119, 4471–4485.
- Gilli, A., Anselmetti, F.S., Ariztegui, D., Bradbury, J.P., Kelts, K.R., Markgraf, V., McKenzie, J.A., 2001. Tracking abrupt climate change in the Southern Hemisphere: a seismic stratigraphic study of Lago Cardiel, Argentina (49 degrees S). *Terra Nova* 13, 443–448.
- González, M.E., Gómez-González, S., Lara, A., Garreaud, R., Díaz-Hormazábal, I., 2018. The 2010–2015 Megadrought and its influence on the fire regime in central and south-central Chile. *Ecosphere* 9, e02300.
- Hale, J.C., Benjamin, J., Woo, K., Astrup, P.M., McCarthy, J., Hale, N., Stankiewicz, F., Wiseman, C., Skriver, C., Garrison, E., Ulm, S., Bailey, G., 2021. Submerged landscapes, marine transgression and underwater shell middens: comparative analysis of site formation and taphonomy in Europe and North America. *Quat. Sci. Rev.* 258, 106867.
- Heaton, T.J., Köhler, P., Butzin, M., Bard, E., Reimer, R.W., Austin, W.E.N., Bronk Ramsey, C., Grootes, P.M., Hughen, K.A., Kromer, B., Reimer, P.J., Adkins, J., Burke, A., Cook, M.S., Olsen, J., Skinner, L.C., 2020. Marine20—the marine radiocarbon age calibration curve (0–55,000 cal BP). *Radiocarbon* 62, 779–820.
- Heiri, O., Lotter, A.F., Lemcke, G., 2001. Loss on ignition as a method for estimating organic and carbonate content in sediments: reproducibility and comparability of results. *J. Paleolimnol.* 25, 101–110.
- Henríquez, C.A., Moreno, P.I., Dunbar, R.B., Mucciarone, D.A., 2021a. The last glacial termination in northwestern Patagonia viewed from the Lago Fonk (~40°S) record. *Quat. Sci. Rev.* 271, 107197.
- Henríquez, C.A., Moreno, P.I., Lambert, F., Alloway, B.V., 2021b. The role of climate and disturbance regimes upon temperate rainforests during the Holocene: a stratigraphic perspective from Lago Fonk (~40°S), northwestern Patagonia. *Quat. Sci. Rev.* 258, 106890.
- Henríquez, W.I., Moreno, P.I., Alloway, B.V., Villarosa, G., 2015. Vegetation and climate change, fire-regime shifts and volcanic disturbance in Chiloé Continental (43°S) during the last 10,000 years. *Quat. Sci. Rev.* 123, 158–167.
- Heusser, C.J., 1966. Late-Pleistocene pollen diagrams from the Province of Llanquihue, southern Chile. *Proc. Am. Phil. Soc.* 110, 269–305.
- Heusser, C.J., 1994. Paleoindians and fire during the late quaternary in southern South-America. *Rev. Chil. Hist. Nat.* 67, 435–443.
- Heusser, C.J., 2003. Ice Age Southern Andes: A Chronicle of Palaeoecological Events. Elsevier Science.
- Heusser, L., Heusser, C., Mix, A., McManus, J., 2006. Chilean and Southeast Pacific paleoclimate variations during the last glacial cycle: directly correlated pollen and δ18O records from ODP Site 1234. *Quat. Sci. Rev.* 25, 3404–3415.
- Higuera, P.E., Brubaker, L.B., Anderson, P.M., Hu, F.S., Brown, T.A., 2009. Vegetation mediated the impacts of postglacial climate change on fire regimes in the south-central Brooks Range, Alaska. *Ecol. Monogr.* 79, 201–219.
- Hogg, A.G., Heaton, T.J., Hua, Q., Palmer, J.G., Turney, C.S.M., Southon, J., Bayliss, A., Blackwell, P.G., Boswijk, G., Bronk Ramsey, C., Pearson, C., Petchey, F., Reimer, P., Reimer, R., Wacker, L., 2020. SHCal20 southern hemisphere calibration, 0–55,000 Years cal BP. *Radiocarbon* 62, 759–778.
- Holz, A., Kitzberger, T., Paritsis, J., Veblen, T.T., 2012. Ecological and climatic controls of modern wildfire activity patterns across southwestern South America. *Ecosphere* 3, 1–25.
- Holz, A., Veblen, T.T., 2009. Pilgerodendron uviferum: the southernmost tree-ring fire recorder species. *Ecoscience* 16, 322–329.
- Holz, A., Veblen, T.T., 2012. Wildfire activity in rainforests in western Patagonia linked to the southern annular mode. *Int. J. Wildland Fire* 21, 114–126.
- Horta, L.R., Marcos, M.A., Sacchi, M., Bozzuto, D.L., Georgieff, S.M., Mancini, M.V., Civalero, M.T., 2019. Paleogeographic and paleoenvironmental evolution in northwestern Santa Cruz (Argentina), and its influence on human occupation dynamics during the late Pleistocene–early Holocene. *Palaeogeogr. Palaeoclimatol. Palaeoecol.* 516, 44–53.
- Huber, U.M., Markgraf, V., Schabitz, F., 2004. Geographical and temporal trends in late quaternary fire histories of fuego-patagonia, south America. *Quat. Sci. Rev.* 23, 1079–1097.
- Iglesias, V., Whitlock, C., 2014. Fire responses to postglacial climate change and human impact in northern Patagonia (41–43°S). *Proc. Natl. Acad. Sci. USA* 111, E5545–E5554.
- Jackson, D., Méndez, C., Aspíllaga, E., 2012. Human remains directly dated to the Pleistocene–Holocene transition support a marine diet for early settlers of the pacific coast of Chile. *J. I. Coast Archaeol.* 7, 363–377.
- Jara, I.A., Moreno, P.I., 2014. Climatic and disturbance influences on the temperate rainforests of northwestern Patagonia (40 °S) since ~14,500 cal yr BP. *Quat. Sci. Rev.* 90, 217–228.
- Jara, I.A., Moreno, P.I., Alloway, B.V., Newnham, R.M., 2019. A 15,400-year long record of vegetation, fire-regime, and climate changes from the northern Patagonian Andes. *Quat. Sci. Rev.* 226, 106005.
- Kean, J.W., Staley, D.M., Cannon, S.H., 2011. In situ measurements of post-fire debris flows in southern California: comparisons of the timing and magnitude of 24 debris-flow events with rainfall and soil moisture conditions. *J. Geophys. Res.: Earth Surf.* 116.
- Krawchuk, M.A., Moritz, M.A., Parisien, M.-A., Van Dorn, J., Hayhoe, K., 2009. Global pyrogeography: the current and future distribution of wildfire. *PLoS One* 4, e5102.
- Garreaud, R., Pezzatti, G.B., Mazzoleni, S., Talbot, L.M., Conedera, M., 2010. Fire regime: history and definition of a key concept in disturbance ecology. *Theor. Biosci.* 129, 53–69.
- Labarca, R., Calás, E., Letelier, J., Alloway, B.V., Holmberg, K., 2021. Arqueología en el Morro Vilcún (Comuna de Chaitén, Región de Los Lagos, Chile): Síntesis y Perspectivas. En Volumen especial que la Sociedad Chilena de Arqueología editará con las actas del Simposio de Adaptaciones Marítimas del Congreso de Arqueología. *Boletín de la Sociedad Chilena de Arqueología* Número Especial, pp. 499–520, 2021.
- Luzio, W., Casanova, M., Seguel, O., 2010. In: Luzio, W. (Ed.), Soils of Chile. University of Chile, Maval Press, Santiago (in Spanish).
- Marcos, M.A., Bamonte, F.P., Echeverría, M.E., Sottile, G.D., Mancini, M.V., 2021. Changes in vegetation and human-environment interactions during the Holocene in the lake pueyrredón area (southern Patagonia). *Veg. Hist. Archaeobotany*.
- Markgraf, V., Anderson, L., 1994. Fire History in Patagonia: Climate versus Human Cause, vol. 1. Revista Instituto de Geología, pp. 35–47.
- Massafarro, J., Laroque-Tobler, I., Brooks, S.J., Vandergoes, M., Dieffenbacher-Krall, A., Moreno, P., 2014. Quantifying climate change in Huemulo mire (Chile, Northwestern Patagonia) during the Last Glacial Termination using a newly developed chironomid-based temperature model. *Palaeogeogr. Palaeoclimatol. Palaeoecol.* 339, 214–224.
- Massafarro, J.J., Moreno, P.I., Denton, G.H., Vandergoes, M., Dieffenbacher-Krall, A., 2009. Chironomid and pollen evidence for climate fluctuations during the last glacial termination in NW Patagonia. *Quat. Sci. Rev.* 28, 517–525.
- McWethy, D.B., Garreaud, R.D., Holz, A., Pederson, G.T., 2021. Broad-scale surface and atmospheric conditions during large fires in south-Central Chile. *Fire* 4, 28.
- McWethy, D.B., Higuera, P.E., Whitlock, C., Veblen, T.T., Bowman, D.M.J.S., Cary, G.J., Haberle, S.G., Kean, R.E., Maxwell, B.D., McGlone, M.S., Perry, G.L.W., Wilmhurst, J.M., Holz, A., Tepley, A.J., 2013. A conceptual framework for predicting temperate ecosystem sensitivity to human impacts on fire regimes. *Global Ecol. Biogeogr.* 22, 900–912.
- Méndez, C., 2013. Terminal Pleistocene/early Holocene 14C dates from archaeological sites in Chile: critical chronological issues for the initial peopling of the region. *Quat. Int.* 301, 60–73.
- Méndez, C., de Porras, M.E., Maldonado, A., Reyes, O., Nuevo Delaunay, A., García, J.-L., 2016. Human effects in Holocene fire dynamics of central western Patagonia (~44° S, Chile). *Frontiers Ecology Evolution* 4.
- Merino-Campos, V., De Pol-Holz, R., Southon, J., Latorre, C., Collado-Fabbri, S., 2019. Marine radiocarbon reservoir age along the Chilean continental margin. *Radiocarbon* 61, 195–210.
- Monnin, E., Indermühle, A., Dännenbach, A., Flückiger, J., Stauffer, B., Stocker, T.F., Raynaud, D., Barnola, J.-M., 2001. Atmospheric CO<sub>2</sub> concentrations over the last glacial termination. *Science* 291, 112–114.
- Montecinos, A., Aceituno, P., 2003. Seasonality of the ENSO-related rainfall variability in Central Chile and associated circulation anomalies. *J. Clim.* 16.
- Moreno, P.I., 2000. Climate, fire, and vegetation between about 13,000 and 9200 C–14 yr BP in the Chilean lake district. *Quat. Res.* 54, 81–89.
- Moreno, P.I., 2004. Millennial-scale climate variability in northwest Patagonia over the last 15000 yr. *J. Quat. Sci.* 19, 35–47.
- Moreno, P.I., 2020. Timing and structure of vegetation, fire, and climate changes on the Pacific slope of northwestern Patagonia since the last glacial termination. *Quat. Sci. Rev.* 238, 106328.
- Moreno, P.I., Alloway, B.V., Villarosa, G., Outes, V., Henríquez, W.I., De Pol-Holz, R., Pearce, N.J.G., 2015a. A past-millennium maximum in postglacial activity from Volcan Chaitén, southern Chile. *Geology* 43, 47–50.
- Moreno, P.I., Denton, G.H., Moreno, H., Lowell, T.V., Putnam, A.E., Kaplan, M.R., 2015b. Radiocarbon chronology of the last glacial maximum and its termination in northwestern Patagonia. *Quat. Sci. Rev.* 122, 233–249.
- Moreno, P.I., Fercovic, E.I., Soteres, R.L., Ugalde, P.I., Sagredo, E.A., Villa-Martinez, R.P., 2022. Glacier and terrestrial ecosystem evolution in the Chilotán archipelago sector of northwestern Patagonia since the Last Glacial Termination. *Earth Sci. Rev.* 235, 104240.
- Moreno, P.I., Francois, J.P., Villa-Martinez, R., Moy, C.M., 2010. Covariability of the southern westerlies and atmospheric CO<sub>2</sub> during the Holocene. *Geology* 39, 727–730.
- Moreno, P.I., Henríquez, W.I., Pescce, O.H., Henríquez, C.A., Fletcher, M.S., Garreaud, R.D., Villa-Martinez, R.P., 2021a. An early Holocene westerly minimum in the southern mid-latitudes. *Quat. Sci. Rev.* 251, 106730.
- Moreno, P.I., Jacobson, G.L., Lowell, T.V., Denton, G.H., 2001. Interhemispheric climate links revealed by a late-glacial cooling episode in southern Chile. *Nature* 409, 804–808.
- Moreno, P.I., Leon, A.L., 2003. Abrupt vegetation changes during the last glacial to Holocene transition in mid-latitude South America. *J. Quat. Sci.* 18, 787–800.
- Moreno, P.I., Videla, J., 2016. Centennial and millennial-scale hydroclimate changes in northwestern Patagonia since 16,000 yr BP. *Quat. Sci. Rev.* 149, 326–337.
- Moreno, P.I., Videla, J., Kaffman, M.J., Henríquez, C.A., Sagredo, E.A., Jara-Arcia, P., Alloway, B.V., 2021b. Vegetation, disturbance, and climate history since the onset of ice-free conditions in the Lago Rosselot sector of Chiloé continental (44°S), northwestern Patagonia. *Quat. Sci. Rev.* 260, 106924.
- Moreno, P.I., Videla, J., Valero-Garcés, B., Alloway, B.V., Heusser, L.E., 2018a. A continuous record of vegetation, fire-regime and climatic changes in northwestern Patagonia spanning the last 25,000 years. *Quat. Sci. Rev.* 198, 15–36.
- Moreno, P.I., Vilanova, I., Villa-Martinez, R., Dunbar, R.B., Mucciarone, D.A., Kaplan, M.R., Garreaud, R.D., Rojas, M., Moy, C.M., Pol-Holz, R.D., Lambert, F.,

- 2018b. Onset and evolution of southern annular mode-like changes at centennial timescale. *Sci. Rep.* 8, 3458.
- Moreno, P.I., Vilanova, I., Villa-Martínez, R.P., Francois, J.P., 2018c. Modulation of fire regimes by vegetation and site type in southwestern Patagonia since 13 ka. *Frontiers Ecology Evolution* 6.
- Moreno, P.I., Villa-Martínez, R., Cardenas, M.L., Sagredo, E.A., 2012. Deglacial changes of the southern margin of the southern westerly winds revealed by terrestrial records from SW Patagonia (52°S). *Quat. Sci. Rev.* 41, 1–21.
- Mottl, O., Flantua, S.G.A., Bhatta, K.P., Felde, V.A., Giesecke, T., Goring, S., Grimm, E.C., Haberle, S., Hooghiemstra, H., Ivory, S., Kuneš, P., Wolters, S., Seddon, A.W.R., Williams, J.W., 2021a. Global acceleration in rates of vegetation change over the past 18,000 years. *Science* 372, 860–864.
- Mottl, O., Grytnes, J.A., Seddon, A.W., Steinbauer, M.J., Bhatta, K.P., Felde, V.A., et al., 2021b. Rate-of-change analysis in paleoecology revisited: a new approach. *Rev. Palaeobot.* 293, 104483.
- Nanavati, W.P., Whitlock, C., Iglesias, V., de Porras, M.E., 2019. Postglacial vegetation, fire, and climate history along the eastern Andes, Argentina and Chile (lat. 41–55°S). *Quat. Sci. Rev.* 207, 145–160.
- Nanavati, W., Whitlock, C., de Porras, M.E., Gil, A., Navarro, D., Neme, G., 2022. Disentangling the last 1,000 years of human-environment interactions along the eastern side of the southern Andes (34–52°S lat.). *Proc. Natl. Acad. Sci. USA* 119, e2119813119.
- Naranjo, J.A., Singer, B.S., Jicha, B.R., Moreno, H., Lara, L.E., 2017. Holocene tephra succession of Puyehue-Cordillera and Antillanca/Casablanca volcanic complexes, southern Andes (40–41°S). *J. Volcanol. Geoth. Res.* 332, 109–128.
- Naranjo, J.A., Stern, C.R., 2004. Holocene tephrochronology of the southernmost part (42°30'–45°S) of the andean southern volcanic zone. *Rev. Geol. Chile* 31, 225–240.
- Oksanen, J., et al., 2019. vegan: Community Ecology Package 732–740, 2020.
- Otero, L., 2006. La huella del fuego. Historia de los bosques nativos y cambios en el paisaje del sur de Chile. Pehuen Editores, Santiago, Chile.
- Palacios, D., Stokes, C.R., Phillips, F.M., Clague, J.J., Alcalá-Reygora, J., Andrés, N., Angel, I., Blard, P.-H., Briner, J.P., Hall, B.L., Dahms, D., Hein, A.S., Jomelli, V., Mark, B.G., Martini, M.A., Moreno, P., Riedel, J., Sagredo, E., Stansell, N.D., Vázquez-Sellem, L., Vuille, M., Ward, D.J., 2020. The deglaciation of the Americas during the last glacial termination. *Earth Sci. Rev.* 203, 103113.
- Perez, S.I., Postillone, M.B., Rindel, D., Gobbo, D., Gonzalez, P.N., Bernal, V., 2016. Peopling time, spatial occupation and demography of Late Pleistocene–Holocene human population from Patagonia. *Quat. Int.* 425, 214–223.
- Pesce, O.H., Moreno, P.I., 2014. Vegetation, fire and climate change in central-east Isla Grande de Chiloé (43°S) since the last glacial maximum, northwestern Patagonia. *Quat. Sci. Rev.* 90, 143–157.
- Pino, M., Abarzúa, A.M., Astorga, G., Martel-Cea, A., Cossío-Montecinos, N., Navarro, R.X., Lira, M.P., Labarca, R., LeCompte, M.A., Adedeji, V., Moore, C.R., Bunch, T.E., Mooney, C., Wolbach, W.S., West, A., Kennett, J.P., 2019. Sedimentary record from Patagonia, southern Chile supports cosmic-impact triggering of biomass burning, climate change, and megafaunal extinctions at 12.8 ka. *Sci. Rep.* 9, 4413.
- Pino, M., Astorga, G.A., 2020. Pilauco: A Late Pleistocene Archaeo-Paleontological Site: Osorno, Northwestern Patagonia and Chile. Springer International Publishing.
- Power, M., Mayle, F., Bartlein, P., Marlon, J., Anderson, R., Behling, H., Brown, K., Carcaillet, C., Colombaroli, D., Gavin, D., Hallett, D., Horn, S., Kennedy, L., Lane, C., Long, C., Moreno, P.I., Paitre, C., Robinson, G., Taylor, Z., Walsh, M., 2013. Climatic control of the biomass-burning decline in the Americas after ad 1500. *Holocene* 23, 3–13.
- Power, M.J., Marlon, J., Ortiz, N., Bartlein, P.J., Harrison, S.P., Mayle, F.E., Ballouche, A., Bradshaw, R.H.W., Carcaillet, C., Cordova, C., Mooney, S., Moreno, P.I., Prentice, I.C., Thonicke, K., Tinner, W., Whitlock, C., Zhang, Y., Zhao, Y., Ali, A.A., Anderson, R.S., Beer, R., Behling, H., Briles, C., Brown, K.J., Brunelle, A., Bush, M., Camill, P., Chu, G.Q., Clark, J., Colombaroli, D., Connor, S., Daniau, A.L., Daniels, M., Dodson, J., Doughty, E., Edwards, M.E., Finsinger, W., Foster, D., Frechette, J., Gaillard, M.J., Gavin, D.G., Gobet, E., Haberle, S., Hallett, D.J., Higuera, P., Hope, G., Horn, S., Inoue, J., Kaltenrieder, P., Kennedy, L., Kong, Z.C., Larsen, C., Long, C.J., Lynch, J., Lynch, E.A., McGlone, M., Meeks, S., Mensing, S., Meyer, G., Minckley, T., Mohr, J., Nelson, D.M., New, J., Newnham, R., Noti, R., Oswald, W., Pierce, J., Richard, P.J.H., Rowe, C., Goni, M.F.S., Shuman, B.N., Takahara, H., Toney, J., Turney, C., Urrego-Sánchez, D.H., Umbanhower, C., Vandergoes, M., Vanniere, B., Vesco, E., Walsh, M., Wang, X., Williams, N., Wilmhurst, J., Zhang, J.H., 2008. Changes in fire regimes since the Last Glacial Maximum: an assessment based on a global synthesis and analysis of charcoal data. *Clim. Dynam.* 30, 887–907.
- Quade, J., Kaplan, M.R., 2017. lake-level stratigraphy and geochronology revisited at Lago (lake) cardiel, Argentina, and changes in the southern hemispheric westerlies over the last 25 ka. *Quat. Sci. Rev.* 177, 173–188.
- Quintana, J.M., Aceituno, P., 2012. Changes in the rainfall regime along the extra-tropical west coast of South America (Chile): 30–43 degrees S. *Atmósfera* 25, 1–22.
- R Core Team, 2022. R: A Language and Environment for Statistical Computing. R Foundation for Statistical Computing, Vienna, Austria. URL.
- Reyes, O., 2020. The Settlement of the Chonos Archipelago, Western Patagonia, Chile. Springer International Publishing.
- Reyes, O., Méndez, C., San Román, M., 2019a. Cronología de la ocupación humana en los canales septentrionales de Patagonia Occidental, Chile. *Intersecc. Antropol.* 20, 87–101.
- Reyes, O., Méndez, C., San Román, M., Francois, J.-P., 2018. Earthquakes and coastal archaeology: assessing shoreline shifts on the southernmost Pacific coast (Chonos Archipelago 43°50'–46°50' S, Chile, South America). *Quat. Int.* 463, 161–175.
- Reyes, O., Moraga, M., Méndez, C., Cherkinsky, A., 2015. Maritime hunter-gatherers in the Chonos archipelago (43°50'–46°50' S), western patagonian channels. *J. I. Coast Archaeol.* 10, 207–231.
- Reyes, O., San Román, M., Morello, F., 2016. Searching for maritime hunter-gatherer archaeological record in the shifting shorelines of the south Pacific coast (Chonos and Guaitecas archipelago, Chile). In: Bjerck, H.B., Breivik, H.M., Fretheim, S.E., Piana, E.L., Skar, B., Tivoli, A.M., Zangrandi, A.F. (Eds.), *Marine Ventures: Archaeological Perspectives on Human–Sea Relations*. Equinox eBooks Publishing, London.
- Reyes, O., Tessone, A., San Román, M., Méndez, C., 2019b. Dieta e isótopos estables de cazadores recolectores marinos en los canales occidentales de Patagonia, Chile. *Lat. Am. Antiq.* 30, 550–568.
- Rick, J.W., 1987. Dates as data: an examination of the Peruvian preceramic radiocarbon record. *Am. Antiqu.* 52, 55–73.
- Rick, T., Ontiveros, M.Á.C., Jerardino, A., Mariotti, A., Méndez, C., Williams, A.N., 2020. Human-environmental interactions in mediterranean climate regions from the Pleistocene to the anthropocene. *Anthropocene* 31, 100253.
- Rodionov, S.N., 2004. A sequential algorithm for testing climate regime shifts. *Geophys. Res. Lett.* 31.
- Romero, J.E., Alloway, B.V., Gutiérrez, R., Bertín, D., Castruccio, A., Villarosa, G., Schipper, C.I., Guevara, A., Bustillos, J., Pisello, A., Daga, R., Montiel, M., Gleeman, E., González, M., Morgavi, D., Ribeiro Guevara, S., Mella, M., 2021. Centennial-scale eruptive diversity at Volcán Calbuco (41.3°S; Northwest Patagonia) deduced from historic tephra cover-bed and dendrochronologic archives. *J. Volcanol. Geoth. Res.* 417, 107281.
- San Román, M., 2014. sea-level changes and coastal peopling in southernmost pacific south America: marine hunters from Patagonia. In: Smith, C. (Ed.), *Encyclopedia of Global Archaeology*. Springer, New York, pp. 6515–6525.
- Sandweiss, D.H., Quilter, J., 2012. Collation, correlation, and causation in the prehistory of coastal Peru. In: Cooper, J., Sheets, P. (Eds.), *Surviving Sudden Environmental Change*. University Press of Colorado, pp. 117–142.
- Sepúlveda-Zúñiga, E., Maidana, N.I., Villacís, L.A., Sagredo, E.A., Moreno, P.I., 2022. The last millennium viewed from a fine-resolution freshwater diatom record from northwestern Patagonia. *Quat. Sci. Rev.* 296, 107806.
- Singer, B.S., Jicha, B.R., Harper, M.A., Naranjo, J.A., Lara, L.E., Moreno-Roa, H., 2008. Eruptive history, geochronology, and magmatic evolution of the Puyehue-Cordillera Caulle volcanic complex, Chile. *Geol. Soc. Am. Bull.* 120, 599–618.
- Smith, R.B., Evans, J.P., 2007. Orographic precipitation and water vapor fractionation over the southern Andes. *J. Hydrometeorol.* 8, 3–19.
- Soil Survey Staff, 2014. Keys to Soil Taxonomy. USDA-Natural Resources Conservation Service, Washington, DC, p. 360.
- Soteres, R.L., Sagredo, E.A., Kaplan, M.R., Martini, M.A., Moreno, P.I., Reynhout, S.A., Schwartz, R., Schaefer, J.M., 2022a. Glacier fluctuations in the northern Patagonian Andes (44°S) imply wind-modulated interhemispheric in-phase climate shifts during Termination 1. *Sci. Rep.* 12, 10842.
- Soteres, R.L., Sagredo, E.A., Moreno, P.I., Lowell, T.V., Alloway, B.V., 2022b. Glacial geomorphology of the central and southern Chilotan Archipelago (42.2°S–43.5°S), northwestern Patagonia. *J. Maps* 1–17.
- Stern, C.R., 2004. Active Andean volcanism: its geologic and tectonic setting. *Rev. Geol. Chile* 31, 161–206.
- Swanson, F.J., Jones, J., Crisafulli, C., González, M.E., Lara, A., 2016. Puyehue-Cordillera Caulle eruption of 2011: tephra fall and initial forest responses in the Chilean Andes. *Bosque* 37, 85–96.
- ter Braak, C.J., Prentice, I.C., 1988. A theory of gradient analysis. In: *Advances in Ecological Research*. Academic Press, pp. 271–317, 18.
- Timpson, A., Barberena, R., Thomas, M.G., Méndez, C., Manning, K., 2021. In: Directly Modelling Population Dynamics in the South American Arid Diagonal Using 14 C Dates, vol. 376. *Philosophical Transactions of the Royal Society B: Biological Sciences*, 20190723.
- Urrutia-Jalabert, R., González, M.E., González-Reyes, Á., Lara, A., Garreaud, R., 2018. Climate variability and forest fires in central and south-central Chile. *Ecosphere* 9, e02171.
- Van Der Werf, G.R., Randerson, J.T., Collatz, G.J., Giglio, L., Kasibhatla, P.S., Arellano, A.F., Olsen, S.C., Kasischke, E.S., 2004. Continental-scale partitioning of fire emissions during the 1997 to 2001 El Niño/La Niña period. *Science* 303, 73–76.
- Villa-Martínez, R., Moreno, P.I., 2021. Development and resilience of deciduous Nothofagus forests since the last glacial termination and deglaciation of the central patagonian Andes. *Palaeogeogr. Palaeoclimatol. Palaeoecol.* 574, 110459.
- Ward, G.K., Wilson, S.R., 1978. Procedures for comparing and combining radiocarbon age determinations: a critique. *Archaeometry* 20, 19–31.
- Whitlock, C., Anderson, R.S., 2003. Fire history reconstructions based on sediment records from lakes and wetlands. In: Veblen, T.T., Baker, W.L., Montenegro, G., Swetnam, T.W. (Eds.), *Fire and Climatic Change in Temperate Ecosystems of the Western Americas*. Springer, New York, pp. 265–295.
- Whitlock, C., Moreno, P.I., Bartlein, P., 2007. Climatic controls of Holocene fire patterns in southern South America. *Quat. Res.* 68, 28–36.
- Williams, A.N., 2012. The use of summed radiocarbon probability distributions in archaeology: a review of methods. *J. Archaeol. Sci.* 39, 578–589.
- Zhang, H., Wang, Z., 2011. Advances in the study of black Carbon effects on climate. *Adv. Clim. Change Res.* 2, 23–30.